

On the spread of changes in marine low cloud cover in climate model simulations of the 21st century

Xin Qu · Alex Hall · Stephen A. Klein ·
Peter M. Caldwell

Received: 3 January 2013 / Accepted: 12 September 2013
© Springer-Verlag Berlin Heidelberg 2013

Abstract In 36 climate change simulations associated with phases 3 and 5 of the Coupled Model Intercomparison Project (CMIP3 and CMIP5), changes in marine low cloud cover (LCC) exhibit a large spread, and may be either positive or negative. Here we develop a heuristic model to understand the source of the spread. The model's premise is that simulated LCC changes can be interpreted as a linear combination of contributions from factors shaping the clouds' large-scale environment. We focus primarily on two factors—the strength of the inversion capping the atmospheric boundary layer (measured by the estimated inversion strength, EIS) and sea surface temperature (SST). For a given global model, the respective contributions of EIS and SST are computed. This is done by multiplying (1) the current-climate's sensitivity of LCC to EIS or SST variations, by (2) the climate-change signal in EIS or SST. The remaining LCC changes are then attributed to changes in greenhouse gas and aerosol concentrations, and other environmental factors. The heuristic model is remarkably skillful. Its SST term dominates, accounting for nearly two-thirds of the intermodel variance of LCC changes in CMIP3 models, and about half in CMIP5 models. Of the two factors governing the SST term (the SST increase and the sensitivity of LCC to SST perturbations), the SST sensitivity drives the spread in the SST term and hence the spread in the overall LCC changes. This sensitivity varies a

great deal from model to model and is strongly linked to the types of cloud and boundary layer parameterizations used in the models. EIS and SST sensitivities are also estimated using observational cloud and meteorological data. The observed sensitivities are generally consistent with the majority of models as well as expectations from prior research. Based on the observed sensitivities and the relative magnitudes of simulated EIS and SST changes (which we argue are also physically reasonable), the heuristic model predicts LCC will decrease over the 21st-century. However, to place a strong constraint, for example on the magnitude of the LCC decrease, will require longer observational records and a careful assessment of other environmental factors producing LCC changes. Meanwhile, addressing biases in simulated EIS and SST sensitivities will clearly be an important step towards reducing intermodel spread in simulated LCC changes.

Keywords Low cloud cover · SST · EIS

1 Introduction

Through their effect on net incoming shortwave radiation, marine low clouds play a critical role in regulating the global energy budget (Hartmann et al. 1992; Klein and Hartmann 1993; Weaver and Ramanathan 1997; Chen et al. 2000). Changes in low clouds associated with simulated anthropogenic climate change likewise typically have a large effect on the shortwave component of the anthropogenic perturbation to the global energy budget (Slingo 1990; Lau et al. 1996; Miller 1997; Larson et al. 1999). These changes play a large role in shaping the response to external forcing seen in climate simulations undertaken in recent decades (Williams et al. 2003, 2006; Stephens 2005;

X. Qu (✉) · A. Hall
Department of Atmospheric and Oceanic Sciences, University of California, PO Box 951565, Los Angeles, CA 90095-1565, USA
e-mail: xinqu@atmos.ucla.edu

S. A. Klein · P. M. Caldwell
Program for Climate Model Diagnosis and Intercomparison,
Lawrence Livermore National Laboratory, Mail Code L-103,
PO Box 808, Livermore, CA 94551, USA

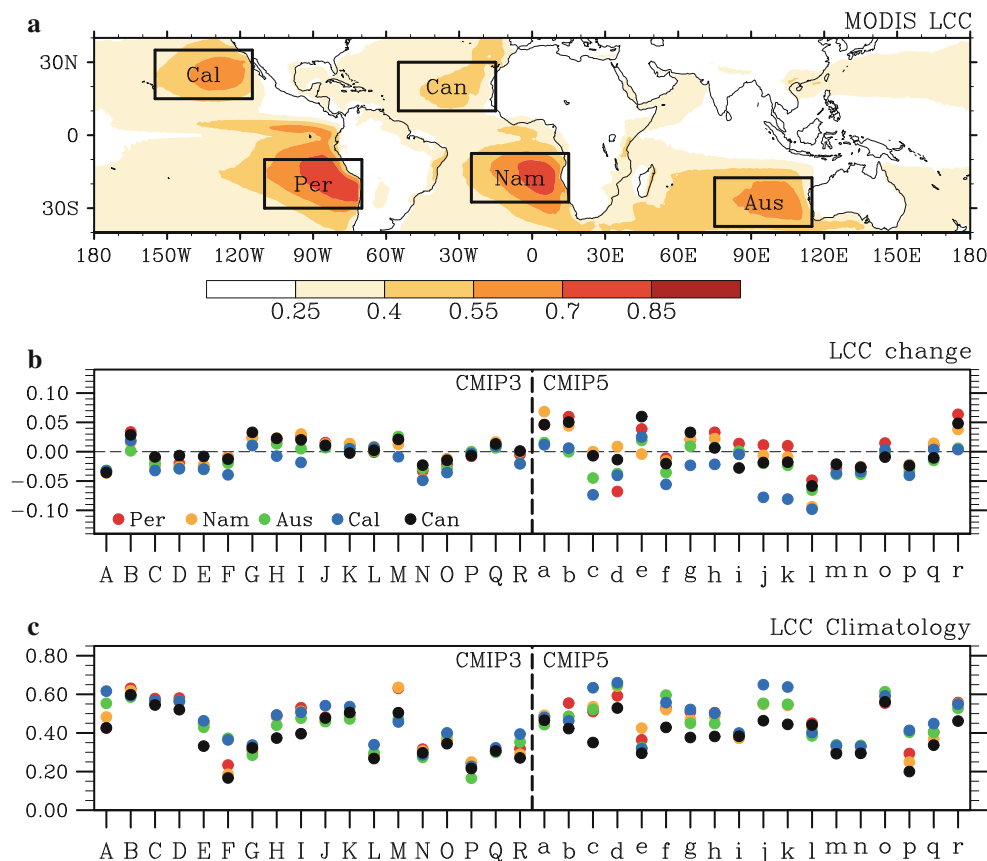


Fig. 1 **a** Geographic distribution of LCC climatology (2000–2010) based on data from the Moderate Resolution Imaging Spectroradiometer (MODIS, King et al. 1992). The main low cloud regions off the coasts of Peru (“Per”), Namibia (“Nam”), Australia (“Aus”), California (“Cal”) and Canary (“Can”) are represented by five black boxes, each of which is 40° by 20°. These regions are used to

construct regional-mean quantities throughout the paper. **b** The 21st-century LCC changes averaged over each of the 5 oceanic regions in 36 models (see Table 1). These changes are computed as differences in the LCC climatologies between the periods 2000–2019 and 2080–2099. **c** Regional-mean LCC climatology (2000–2019) in the 5 oceanic regions and 36 models

Wyant et al. 2006). They also exhibit a large spread across models (Cess et al. 1990; Colman 2003; Bony and Dufresne 2005; Bony et al. 2006; Soden and Held 2006; Webb et al. 2006; Dufresne and Bony 2008; Medeiros et al. 2008; Zelinka et al. 2012). A sizeable portion of the spread originates in the subtropical stratocumulus regions off the west coasts of continents (Soden and Vecchi 2011; Webb et al. 2012, references therein). In these regions, simulated changes in low cloud cover (LCC) vary a great deal in sign and magnitude across models (Stephens 2005; Zhang and Bretherton 2008; Briant and Bony 2012; and see also Fig. 1 of this study).

Simulated LCC changes in the stratocumulus regions are likely driven by changes in their large-scale environment. The goal of this study is to determine what these large-scale environmental changes are, and assess their relative importance to the intermodel spread in LCC changes. Many studies (Klein and Hartmann 1993; Bretherton and Wyant 1997; Miller 1997; Larson et al. 1999; Wood and Bretherton 2006; Clement et al. 2009; Sun et al. 2011;

Chung and Teixeira 2012; Caldwell et al. 2013; Rieck et al. 2012; Watanabe et al. 2012) identify two thermodynamical variables as the most important large-scale controls on LCC: One is the strength of the inversion that caps the planetary boundary layer (PBL). The other variable is sea surface temperature (SST).

In the case of the inversion strength, the physical argument for a link to LCC is the following: A stronger inversion suppresses the mixing of boundary layer air with warmer and drier air in the free-troposphere, leading to a shallower, moister and cloudier PBL. There is ample observational evidence for a link between inversion strength and low cloud cover. Seasonal and interannual LCC variations in many low cloud regions are strongly associated with variations in this quantity (Slingo 1980; Klein and Hartmann 1993; Wood and Bretherton 2006; Sun et al. 2011). If the inversion strength indeed increases in climate change, as suggested by several studies (Miller 1997; Larson et al. 1999; Caldwell et al. 2013, and as we find here in this study), and if LCC changes are dominated

by the PBL moistening induced by this increase, then LCC would increase. In this study, to measure inversion strength, we adopt the estimated inversion strength (EIS), a quantity constructed by Wood and Bretherton (2006).

In the case of SST, an increase in SST with no changes in the inversion strength may lead to a relatively drier and less cloudy PBL. Two mechanisms that would lead to such a relationship have emerged in recent modeling studies: First, surface warming increases surface latent heat flux, enhancing mixing of boundary layer air with warmer and drier air aloft (Bretherton and Wyant 1997; Chung and Teixeira 2012; Rieck et al. 2012). Second, through its effect on surface moisture flux, surface warming increases the contrast between the moisture content of the boundary layer and that of free-tropospheric air, so the mixing with the free-tropospheric air has a stronger drying effect on the boundary layer air as SST increases (Brient and Bony 2012). If LCC feedback is dominated by the surface-warming-induced PBL drying, then LCC would decrease.

In addition to EIS and SST, many other factors such as subsidence, horizontal advection, free-tropospheric humidity and greenhouse gas (GHG) and aerosol concentrations are also considered to be important to low clouds (Albrecht 1989; Bretherton and Wyant 1997; Lohmann and Feichter 2001; Norris 2001; Vecchi et al. 2006; Gregory and Webb 2008; Zhang and Bretherton 2008; Andrews et al. 2012; Watanabe et al. 2012; Caldwell et al. 2013; Chung and Teixeira 2012).

To sort through all this potential complexity, we start with the working hypothesis that EIS and SST are the most important factors shaping the LCC response in simulated future climate change (However, we do not exclude the possibility that other factors are important as well, and where possible, we quantify their importance.). We also assume simulated LCC changes in global models can be interpreted as a linear combination of the contributions from all the controls. Accordingly, we develop a heuristic model designed to tease out each contribution. In this heuristic model, the contribution from each thermodynamical variable (EIS or SST) is quantified by the product of anthropogenic change in that variable and a local LCC sensitivity to it. LCC changes not linearly attributable to either EIS or SST changes (the residual term) are then attributed to changes in other cloud-controlling factors. It is possible EIS and SST affect LCC in a nonlinear fashion. Such nonlinear effects are also included in the residual term. The global models whose LCC changes we are trying to interpret are 18 climate models participating in phase 3 of the Coupled Model Intercomparison Project (CMIP3, see Table 1) and 18 climate models participating in phase 5 of the Coupled Model Intercomparison Project (CMIP5, see Table 1). Our regions of interest are five subtropical stratocumulus regions, defined by black boxes in Fig. 1a.

The heuristic model requires anthropogenic changes in EIS and SST, as well as local LCC sensitivities to these variables, for each of the models, and each of the regions. While it is straightforward to quantify simulated anthropogenic changes in EIS and SST, it is not obvious how to quantify the simulated LCC sensitivities. In this study, we assume the EIS and SST sensitivities informing the heuristic model can be derived from interannual climate variability. This assumption allows us to quantify the sensitivities based on simulated interannual climate variability in the 20th-century. If simulated LCC changes turn out to be strongly influenced by the sensitivities, this then creates a path towards an observational constraint of LCC changes. The simulated sensitivities calculated from current climate can be compared to their observed counterparts, and unrealistic responses can be identified. In this study, we also quantify the respective contributions of GHG and aerosol by examining several idealized simulations with prescribed changes in GHG and aerosol concentrations.

Previous studies have demonstrated the importance of PBL and cloud parameterizations in shaping the cloud response to external forcing (Mitchell et al. 1989; Senior and Mitchell 1993; Yao and Del Genio 1999; Medeiros and Stevens 2011). In this study, we also explore to what extent the intermodel spread in LCC changes are linked to differences in the models' PBL and cloud parameterizations. We categorize the parameterizations into different types based on their key features. We then examine the behavior of model sub-ensembles corresponding to the various parameterization categories, and assess whether these model sub-ensembles are distinctively different in the sign and magnitude of simulated LCC changes. This turns out to be the case, allowing us to then use the heuristic model to understand better the influence of the parameterizations. The elements of the heuristic model most directly influenced by the parameterizations are the local sensitivities to EIS and SST changes, so these are the focus of our investigation.

The study is presented as follows: Data and methodology are described in Sect. 2. Anthropogenic changes in LCC, EIS and SST are presented in Sect. 3, and local EIS and SST sensitivities in Sect. 4. Various contributions to the LCC changes and their relative importance to the intermodel spread are assessed in Sect. 5. The link between parameterization and the LCC changes is examined in Sect. 6. The realism of simulated EIS and SST sensitivities are assessed against observed EIS and SST sensitivities in Sect. 7. A summary and discussions are found in Sect. 8.

2 Data and methodology

20th- and 21st-century climates simulated by 36 CMIP3 and CMIP5 models (see Table 1) are examined. Historical

Table 1 Thirty-six CMIP models used in this study

Letter	Model	PBL scheme	Cloud scheme	Reference
A	BCCR-BCM2.0	<i>K</i> (Ri)	Diag (PDF)	Déqué et al. (1994)
B*	CCSM3	<i>K</i> profile	Diag (RH, stability)	Collins et al. (2004)
C	CGCM3.1(T47)	<i>K</i> (Ri)	Diag (RH, stability)	Scinocca et al. (2008)
D	CGCM3.1(T63)	<i>K</i> (Ri)	Diag (RH, stability)	Scinocca et al. (2008)
E	CSIRO-Mk3.5	<i>K</i> (Ri)	Diag (PDF)	Gordon et al. (2002)
F	ECHAM5/MPI-OM	<i>K</i> (TKE)	Diag (PDF)	Roeckner et al. (2003)
G*	FGOALS-g1.0	<i>K</i> profile	Diag (RH, stability)	Yu et al. (2004)
H'	GFDL-CM2.0	<i>K</i> profile	Prog	Delworth et al. (2006)
I'	GFDL-CM2.1	<i>K</i> profile	Prog	Delworth et al. (2006)
J	GISS-EH	<i>K</i> (TKE)	Diag (RH, stability)	Schmidt et al. (2006)
K	GISS-ER	<i>K</i> (TKE)	Diag (RH, stability)	Schmidt et al. (2006)
L	INGY-SXG	<i>K</i> (TKE)	Diag (RH)	Roeckner et al. (1996)
M	INM-CM3.0	<i>K</i> (Ri)	Diag (RH, stability)	Volodin and Diansky (2004)
N	IPSL-CM4	<i>K</i> (Ri)	Diag (PDF)	Hourdin et al. (2006)
O	MIROC3.2(medres)	<i>K</i> (Ri)	Diag (PDF)	K-1 model developers (2004)
P	MRI-CGCM2.3.2	<i>K</i> (Ri)	Diag (RH)	Yukimoto et al. (2001)
Q*	PCM	<i>K</i> profile	Diag (RH, stability)	Washington et al. (2000)
R	UKMO-HadCM3	<i>K</i> (Ri)	Diag (PDF)	Gordon et al. (2000)
a*	BCC-CSM1.1	<i>K</i> profile	Diag (RH, stability)	Wu et al. (2010)
b*	CCSM4	<i>K</i> profile	Diag (RH, stability)	Neale et al. (2010)
c	CSIRO-Mk3.6	<i>K</i> (Ri)	Diag (PDF)	Rotstayn et al. (2010)
d	CanESM2	<i>K</i> (Ri)	Diag (RH, stability)	Chylek et al. (2011)
e*	FGOALS-s2	<i>K</i> (TKE)	Diag (RH, stability)	Bao et al. (2013)
f'	GFDL-CM3	<i>K</i> profile	Prog	Donner et al. (2011)
g'	GFDL-ESM2G	<i>K</i> profile	Prog	Dunne et al. (2012)
h'	GFDL-ESM2M	<i>K</i> profile	Prog	Dunne et al. (2012)

Table 1 continued

Letter	Model	PBL scheme	Cloud scheme	Reference
i	GISS-E2-R	<i>K</i> (TKE)	Diag (RH, stability)	Schmidt et al. (2013)
j'	HadGEM2-CC	<i>K</i> profile	Diag (PDF)	Martin et al. (2011)
k'	HadGEM2-ES	<i>K</i> profile	Diag (PDF)	Martin et al. (2011)
l	IPSL-CM5A-LR	<i>K</i> (Ri)	Diag (PDF)	Dufresne et al. (2013)
m	MIROC-ESM	<i>K</i> (Ri)	Diag (PDF)	Watanabe et al. (2011)
n	MIROC-ESM-CHEM	<i>K</i> (Ri)	Diag (PDF)	Watanabe et al. (2011)
o	MIROC5	<i>K</i> (TKE)	Diag (PDF)	Watanabe et al. (2010)
p	MPI-ESM-LR	<i>K</i> (TKE)	Diag (RH)	Stevens et al. (2013)
q	MRI-CGCM3	<i>K</i> (Ri)	Diag (PDF)	Yukimoto et al. (2011)
r*	NorESM1-M	<i>K</i> profile	Diag (RH, stability)	Bentsen et al. (2012)

1st column: Reference letters of 18 CMIP3 (upper case) and 18 CMIP5 models (lower case). 2nd column: Names of the models. 3rd column: Categorization of PBL parameterizations in the models. It is based on how the PBL eddy diffusivity is parameterized. Models that use cloud-top radiative cooling to drive boundary layer turbulence are also identified by the prime in the first column. 4th column: Categorization of cloud cover parameterizations. Diagnostic and prognostic schemes are referred to as “Diag” and “Prog”, respectively. Relative humidity and the stability of the atmosphere are denoted as RH and stability for simplicity. A subset of models in the “Diag (RH, stability)” category, in which the Slingo-type cloud scheme or its variant is used, are identified by the asterisk in the first column. 5th column: References are provided for each model

forcing was imposed in the 20th-century simulations, which in the case of the CMIP5 models end in 2005 rather than 2000. In the 21st-century simulations, the anthropogenic forcing scenario A1B (Nakićenović et al. 2000) was imposed on the CMIP3 models, while the Representative Concentration Pathways (RCP) 8.5 (Taylor et al. 2012) was imposed on the CMIP5 models. By construction, the RCP 8.5 constitutes slightly stronger radiative forcing than the scenario A1B: Radiative forcing between the periods 2000–2019 and 2080–2099 is about 4.1 Wm^{-2} for the scenario A1B and 5.3 Wm^{-2} for the RCP 8.5. The projected evolution of aerosol concentrations in the 21st century also differs between the scenario A1B and the RCP 8.5: Concentrations in most aerosol compositions increase in the scenario A1B, while they decrease in the RCP 8.5.

LCC is defined as the overall cloud cover below 680 hPa, a definition also used in the International Satellite Cloud Climatology Project (ISCCP, Rossow and Schiffer

1991). Random overlapping is assumed to obtain the overall cloud cover from cloud fraction at multiple vertical levels. EIS is defined as in Wood and Bretherton (2006):

$$EIS = LTS - \Gamma_m^{850} \cdot (z_{700} - LCL) \tag{1}$$

where *LTS* is the lower-tropospheric stability, defined as the difference in potential temperature between 700 hPa and the surface, Γ_m^{850} is the moist-adiabatic potential temperature gradient at 850 hPa, which is in turn a function of the 850 hPa temperature, z_{700} is the height of the 700 hPa surface, and *LCL* is the lifting condensation level. Consistent with Wood and Bretherton (2006), we approximate the 850 hPa temperature by the mean of the 700 hPa and surface temperatures.

To generate input for the heuristic model, we first compute simulated changes over the 21st century in the regionally-averaged annual-mean LCC, EIS and SST (respectively: ΔLCC , ΔEIS and ΔSST) in five oceanic regions, defined by the ocean portions of the black boxes in Fig. 1a. These changes are computed as differences in the climatologies of these quantities between the periods 2000–2019 and 2080–2099. Our heuristic model expresses simulated LCC changes as:

$$\Delta LCC = \frac{\partial LCC}{\partial EIS} \cdot \Delta EIS + \frac{\partial LCC}{\partial SST} \cdot \Delta SST + R \tag{2}$$

where the partial derivatives $\partial LCC / \partial EIS$ and $\partial LCC / \partial SST$ represent the sensitivities of LCC to these two variables. We compute these sensitivities based on simulated inter-annual climate variability in the 20th-century as follows. (Here, interannual climate variability refers to variability on times scales longer than a year, but shorter than a century.) First, we remove the long-term trend from each of the LCC, EIS and SST time series. Then we regress the LCC time series onto either the EIS or SST series. A complicating factor is that EIS and SST time series are not independent. For example, an increase in SST is often associated with a decrease in EIS. To eliminate the potential ambiguity of EIS-SST covariance in the $\partial LCC / \partial EIS$ estimate, we remove the components of LCC and EIS variations that are linearly related to SST variations by regression analysis before then regressing LCC onto EIS. Likewise, we remove the components of LCC and SST variations that are linearly related to EIS variations before estimating $\partial LCC / \partial SST$. (A detailed description on how these sensitivities are calculated is given in “Appendix 1”.) To examine the robustness of our estimates, we also compute $\partial LCC / \partial EIS$ and $\partial LCC / \partial SST$ based on the pre-industrial control simulations and 21st-century simulations (scenario A1B for CMIP3 models and RCP 8.5 for CMIP5 models) with the 36 models. These simulations generally yield very similar LCC sensitivities to the corresponding historical simulations (see

“Appendix 1”). For simplicity, $\partial LCC / \partial EIS$ and $\partial LCC / \partial SST$ are also referred hereafter to as the EIS and SST slopes. The total contribution of EIS to the LCC change is represented by the first term on the right side of Eq. (2), and the contribution of SST is represented by the second term. The last term on the right side of Eq. (2), *R* represents the residual LCC changes, namely, LCC changes that cannot be attributed in a linear fashion to either EIS or SST changes, and is calculated as the value that makes the equality in (2) true. In this work, the heuristic model, Eq. (2) is used as an exploratory tool to uncover and understand the behaviors of LCC responses in 36 climate simulations.

We estimate the direct contribution of the anthropogenic increase in GHG concentration to simulated LCC changes in eight CMIP5 models in three steps. (In this work, the direct GHG contribution refers to LCC changes induced by GHG-forced environmental changes other than changes in EIS and SST. It is closely linked to the so-called “cloud fast response” discovered by Gregory and Webb (2008).) First, we examine the CO₂ quadrupling simulations (“sstClim4xCO₂”) done with eight Atmospheric General Circulations Models (AGCMs) and their corresponding control simulations (“sstClim”). (These AGCMs are the atmospheric components of eight fully coupled atmosphere-ocean models in the CMIP5 archive listed in Table 1. For convenience, we refer to them by the reference letters of their corresponding coupled models.) These two types of simulations are run with the same SST climatology, but different CO₂ concentrations for a 30-year period. The “sstClim” simulations are run with the pre-industrial CO₂ concentration, while the “sstClim4xCO₂” simulations are run with the CO₂ concentration that is four times the pre-industrial level. The apparent effect of the CO₂ quadrupling on LCC is quantified by the difference in LCC climatologies between these simulations. It turns out there is a robust EIS increase in the “sstClim4xCO₂” simulations. The EIS increase averaged over the 5 regions and the eight AGCM simulations is about 0.4 K. This suggests that the LCC changes from the “sstClim” to “sstClim4xCO₂” simulations contain not only the direct effect of the CO₂ increase, but also some contribution from the EIS increase. (The SST contribution in these simulations vanishes by construction.) So, in the second step, we quantify the contribution of the EIS increase using the EIS slope obtained from the historical simulations ($\Delta EIS \cdot \partial LCC / \partial EIS$) and remove it from the overall LCC changes. The resultant LCC change then represents the direct effect of the CO₂ quadrupling to LCC. Finally, to account for the fact that the CO₂-equivalent radiative forcing corresponding to the RCP 8.5 (5.3 Wm⁻²) is about 30 % smaller than radiative forcing corresponding to the CO₂ quadrupling (7.4 Wm⁻²), we rescale the estimated CO₂ effect proportionally.

To estimate the direct contribution of aerosol (in isolation from any EIS and SST contributions) to simulated LCC changes, we examine the aerosol loading simulations (“sstClimAerosol”) done with eight AGCMs. (These AGCMs are precisely the ones used to estimate the direct CO₂ effect.) The “sstClimAerosol” simulations differ from their control simulations (“sstClim”) only in their imposed aerosol concentrations or emissions in the case of models with interactive aerosols. The “sstClim” simulations are run with the pre-industrial aerosols, while the “sstClim-Aerosol” simulations are run with aerosols in 2000. There is a general increase in aerosol concentrations in 2000 compared to the pre-industrial period. The net effect of the aerosol increase on LCC is quantified by the difference in LCC climatologies between the “sstClim” and “sstClim-Aerosol” simulations. (EIS changes little in the “sstClim-Aerosol” simulations.) To account for the fact that aerosol concentrations in the RCP 8.5 simulations decrease in the 21st century, we flip the sign of the estimated aerosol effect. Note that the magnitude of the aerosol decrease in RCP 8.5 is comparable to the magnitude of the aerosol increase from the pre-industrial period to 2000, so there is no need to rescale the estimated aerosol effect.

To estimate observed EIS and SST slopes, we use IS-CCP cloud data (Rossow and Schiffer 1991), ERA-Interim reanalysis (Dee et al. 2011) and NOAA optimum interpolation monthly SST version 2 (Reynolds et al. 2002) during the period 1984–2009. To correct the known error of IS-CCP assigning low-clouds under strong inversions to middle clouds (see Garay et al. 2008; Sun et al. 2011), we estimate LCC as follows: $LCC = (L + M)/(1 - H)$, where L, M and H are respectively: low, middle and high cloud amount given in the ISCCP data.

3 Assessing 21st-century changes in LCC, EIS and SST

3.1 LCC

Simulated LCC changes over the 21st-century in the 5 subtropical oceanic regions and 36 models are shown in Fig. 1b. Not surprisingly, in every region, the sign of the LCC changes varies from model to model: It is positive as often as it is negative. In contrast, the sign of the LCC changes in any particular model is largely consistent across the regions. This suggests that in any particular model, typically there are anthropogenic changes in the large-scale atmospheric environment common to all the regions. Interestingly, there is virtually no correspondence between the LCC change and LCC climatology, a fact easily discernible by visually examining Fig. 1b, c, and confirmed by calculations of correlation (0.08 for CMIP3 models and –0.02 for CMIP5 models). From this information, we infer

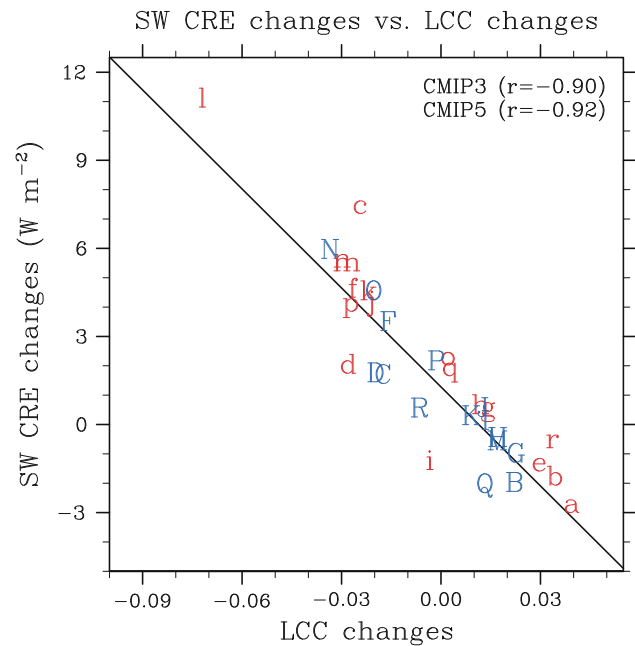


Fig. 2 Scatterplot of changes in SW CRE averaged over the 5 oceanic regions versus LCC changes averaged over the 5 oceanic regions in 18 CMIP3 and 18 CMIP5 models. CMIP3 models are color-coded in blue, and CMIP5 models in red. Three CMIP3 models (A, E and L) are not shown because they do not have necessary data available to perform this calculation. Solid line represents a least-squares fit regression line based on all models

that the LCC climatology is not helpful in understanding controls on LCC changes.

Averaged over all the regions, the LCC changes range from –0.04 to 0.02 in CMIP3 models and –0.07 to 0.04 in CMIP5 models. The spread in LCC changes is larger in the CMIP5 ensemble because of larger EIS and SST increases (see the discussion below). To quantify the climatic impact of these changes, we compute simulated changes in shortwave (SW) cloud radiative effect (CRE) over the 21st-century in the 5 oceanic regions and 36 models. (SW CRE is defined as the difference between the clear- and all-sky net incoming solar radiation at the top of atmosphere.) Figure 2 scatters changes in SW CRE averaged over all the regions vs. the corresponding averages of LCC changes in the 36 models. Changes in SW CRE are strongly anticorrelated with LCC changes across both ensembles with correlations of about –0.90. Thus about 80% of the intermodel variance of SW CRE changes is accounted for by LCC changes. Consistent with Zelinka et al. (2012), changes in LCC, as opposed to optical depth, are dominant in explaining effects of anthropogenic cloud changes on absorbed shortwave radiation for subtropical boundary layer cloud regions. Regression analysis yields a sensitivity of about 1 W m^{-2} for a 0.01 change in LCC, similar to observed (Klein and Hartmann 1993). Based on this number and simulated LCC changes, we estimate the range

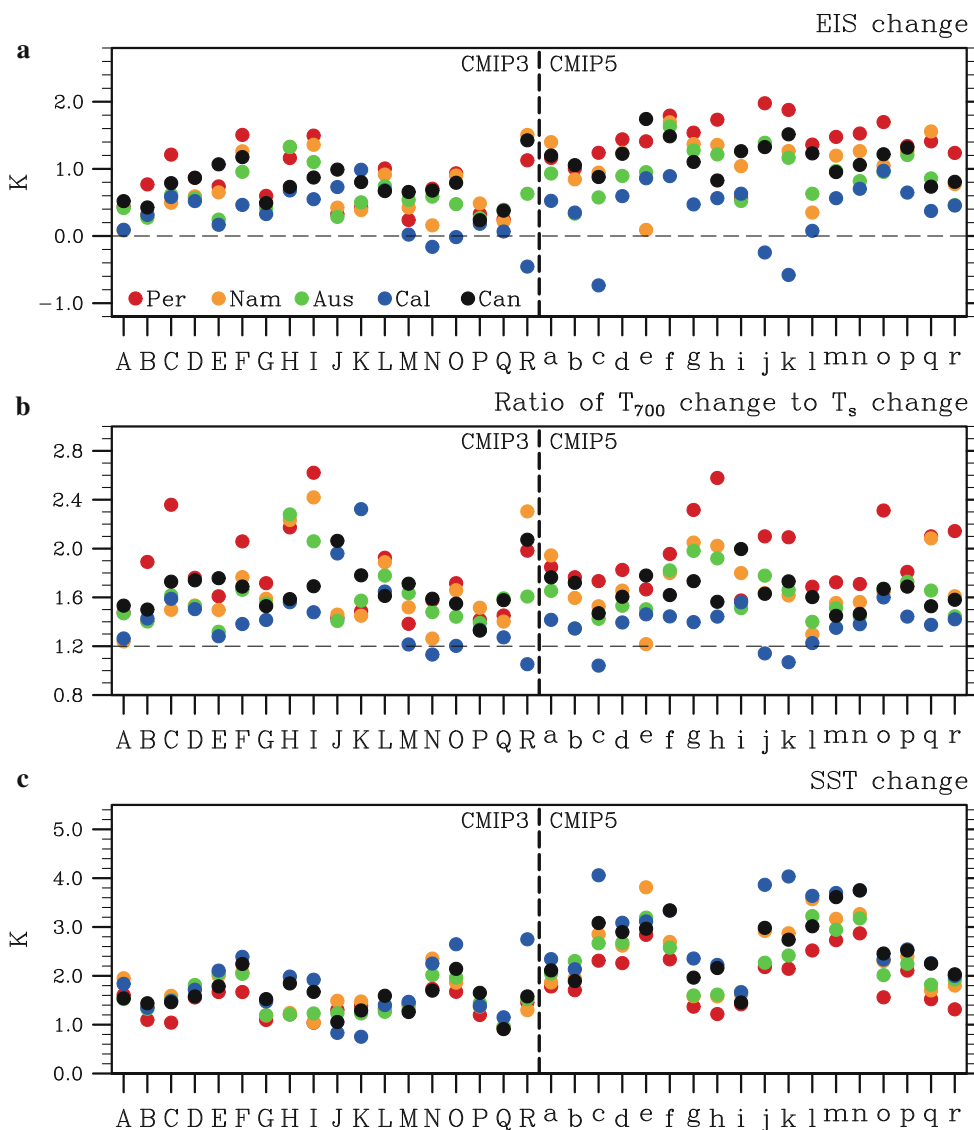


Fig. 3 **a** EIS change, **b** the ratio of T_{700} change to T_s change and **c** SST change in the 5 oceanic regions and 36 models. Dashed line in **b** represents $\Delta T_{700}/\Delta T_s = 1.2$

of SW radiative perturbations induced by the LCC changes to be -2 to 4 W m^{-2} in the CMIP3 models and -4 to 7 W m^{-2} in the CMIP5 models.

3.2 EIS

EIS changes in the 5 oceanic regions and 36 models are shown in Fig. 3a. There is a systematic increase in EIS in a warming climate across models and regions. The ensemble-mean change in EIS, averaged across the regions, is 0.62 K for the CMIP3 models and about 1 K for the CMIP5 models (Table 2). The only exceptions are the EIS changes in some models over the Californian region (blue circles). In these cases, no increase or even a slight decrease in EIS is seen. Interestingly, the Californian region is also the region with

the least EIS increase in most models. Likewise, the Peruvian region typically has the greatest increase in EIS. In spite of the general EIS increase across models and regions, the magnitude of the EIS change varies considerably from model to model. The intermodel standard deviation of the EIS change averaged over the 5 regions is about 0.2–0.3 K across either the CMIP3 or CMIP5 ensemble (Table 2). Note that relative to the ensemble-mean, the intermodel spread in the EIS change is much smaller in the CMIP5 ensemble than in CMIP3 (22 vs. 44 %).

Next we explore the origins of the simulated EIS changes. Starting from the definition of EIS in Eq. (1), and making some valid assumptions (see “Appendix 2” for detail), we can derive the EIS change (ΔEIS) as a linear combination of warming at the 700 hPa (ΔT_{700}) and the surface (ΔT_s):

Table 2 EIS and SST changes and EIS and SST slopes in 36 CMIP models

	CMIP3	CMIP5
EIS change	0.62 (0.27)	1.01 (0.22)
SST change	1.54 (0.32)	2.48 (0.61)
EIS slope	1.14 (1.33)	1.52 (1.66)
SST slope	-1.14 (1.08)	-1.15 (1.00)

1st row: The ensemble-mean of EIS changes averaged over the 5 regions in 18 CMIP3 and 18 CMIP5 models. 2nd row: As in the 1st row, but for SST changes. 3rd row: As in the 1st row, but for EIS slopes. 4th row: As in the 1st row, but for SST slopes. The intermodel standard deviation of all quantities are shown in parentheses. Unit for EIS and SST changes is K and 0.01 K^{-1} for EIS and SST slopes

$$\Delta EIS \approx \alpha \cdot \Delta T_{700} - \beta \cdot \Delta T_s \quad (3)$$

where $\alpha = 0.97$ and $\beta = 1.14$. (Regressing ΔEIS in all regions and all models against the corresponding values for ΔT_{700} and ΔT_s yields diagnosed values of α and β that are very similar: 1.0 and 1.2.) Using simulated values for ΔT_{700} , ΔT_s , and ΔEIS from all models and our 5 regions, we find that the right-hand side of Eq. (3) is almost perfectly correlated with the left-hand side ($r = 0.99$). The standard error of the right side of Eq. (3) in representing ΔEIS is about 0.05, at least one order of magnitude smaller than ΔEIS in almost all the cases. Since Eq. (3) captures ΔEIS so well, we use it to understand controls on simulated EIS changes.

According to Wood and Bretherton (2006), if the vertical profile of tropospheric warming followed a moist adiabat from the subtropical surface, $\Delta T_{700}/\Delta T_s \approx 1.2$ and ΔEIS vanishes (also consistent with Eq. 3). However, in more than 90 % of the cases, the simulated values of $\Delta T_{700}/\Delta T_s$ are greater than 1.2 (see Fig. 3b). This suggests that subtropical warming just above the boundary layer is generally greater than the moist adiabat from the surface would imply, given surface warming. This greater-than-adiabatic warming in the subtropical free-troposphere is precisely what drives the systematic increase in EIS seen in Fig. 3a.

The question now arises: Why does the subtropical lower-troposphere warm superadiabatically? The answer to this question may lie in two robust features of climate change. One is that warming in tropical warm pools (one such region is represented by black boxes in Figs. 4, 5) is greater than warming in low cloud regions (see Liu et al. 2005 for more discussions on this phenomenon). To demonstrate that, we examine the geographic distributions of the ensemble-mean surface temperature change in Fig. 4. Indeed, in both CMIP3 and CMIP5 ensembles, the warm pools warm more than the low cloud regions. Since free tropospheric tropical temperatures are largely set by SST in the warm pools, the greater warming in the warm pools contributes to simulated superadiabatic warming and hence the EIS increases in the low cloud regions. The other is that

warming over nearby land is generally greater than warming in the low cloud regions (Fig. 4, see also Sutton et al. 2007). This could enhance warming in the free-troposphere in the low cloud regions through episodic advection of warmer air from the continents to the marine stratocumulus regions immediately to the west. To demonstrate that, we examine the geographic distributions of the ensemble-mean T_{700} change (Fig. 5). Indeed, in both CMIP3 and CMIP5 ensembles, the low cloud regions exhibit enhanced warming in the free troposphere closer to the values over the nearby continents, contributing to simulated EIS increases. Further work would be necessary to quantitatively establish the contribution of these mechanisms to the EIS increases seen in Fig. 3a.

3.3 SST

SST changes in the 5 oceanic regions and 36 models are shown in Fig. 3c. The ensemble-mean of the changes averaged across the regions is about 1.54 K in CMIP3 models and 2.48 K in CMIP5 models (Table 2). Greater surface warming in CMIP5 models scales approximately with the greater radiative forcing in RCP 8.5. The intermodel standard deviations of the EIS and SST changes are also shown in Table 2. We note that EIS and SST changes are not significantly correlated to one another across either the CMIP3 or CMIP5 ensemble.

4 EIS and SST slopes

The EIS slopes ($\partial LCC/\partial EIS$) in the 5 oceanic regions and 36 models calculated from 20th-century variability are shown in Fig. 6a. They are positive in more than 80 % of the cases, indicating increasing LCC with increasing EIS. This simulated co-variability of LCC and EIS from year to year is qualitatively consistent with the observed relationship between the two variables based on the seasonal cycle, regional variations, and interannual variability (Klein and Hartmann 1993; Wood and Bretherton 2006; Sun et al. 2011). The SST slope ($\partial LCC/\partial SST$), as shown in Fig. 6b, is negative in about 80 % of the cases, generally indicating decreasing LCC with increasing SST. This is also qualitatively consistent with the physical argument for the SST-LCC relationship put forward in the introduction. The ensemble-mean EIS and SST slope averaged over all the regions are given in Table 2. Though their signs generally agree, the magnitudes of both EIS and SST slopes vary significantly from model to model (Fig. 6a, b; Table 2). Note that EIS and SST slopes are not significantly correlated one another across either CMIP3 or CMIP5 models. Comparison of these slopes to observations is shown in Sect. 7.

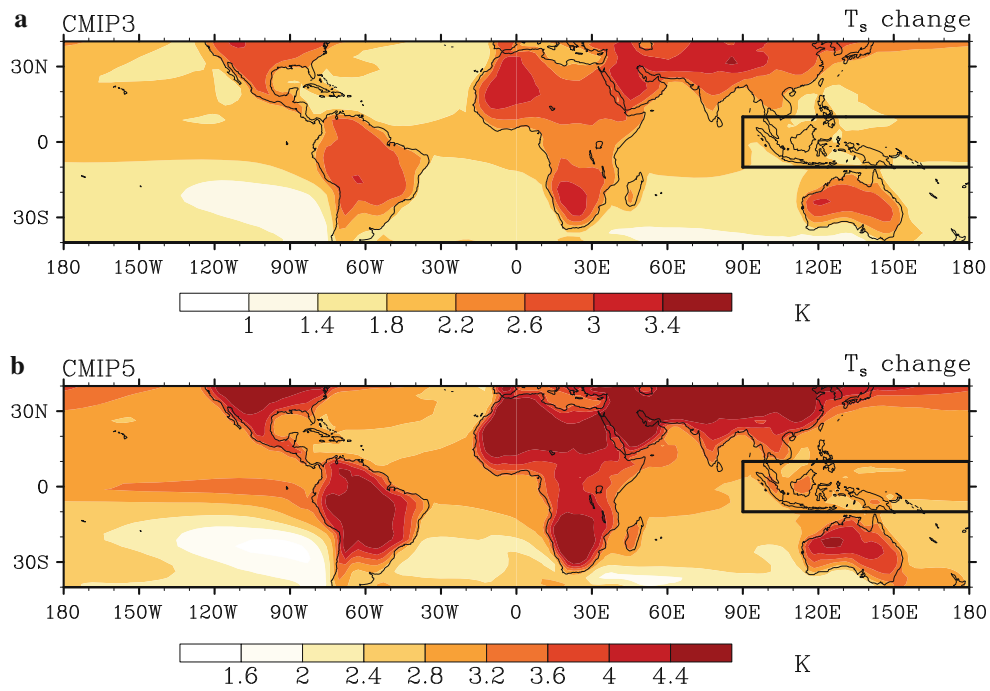


Fig. 4 Geographic distributions of **a** CMIP3 and **b** CMIP5 ensemble-mean surface temperature change. The approximate location of the western Pacific warm pool is represented by the *black box* in each diagram

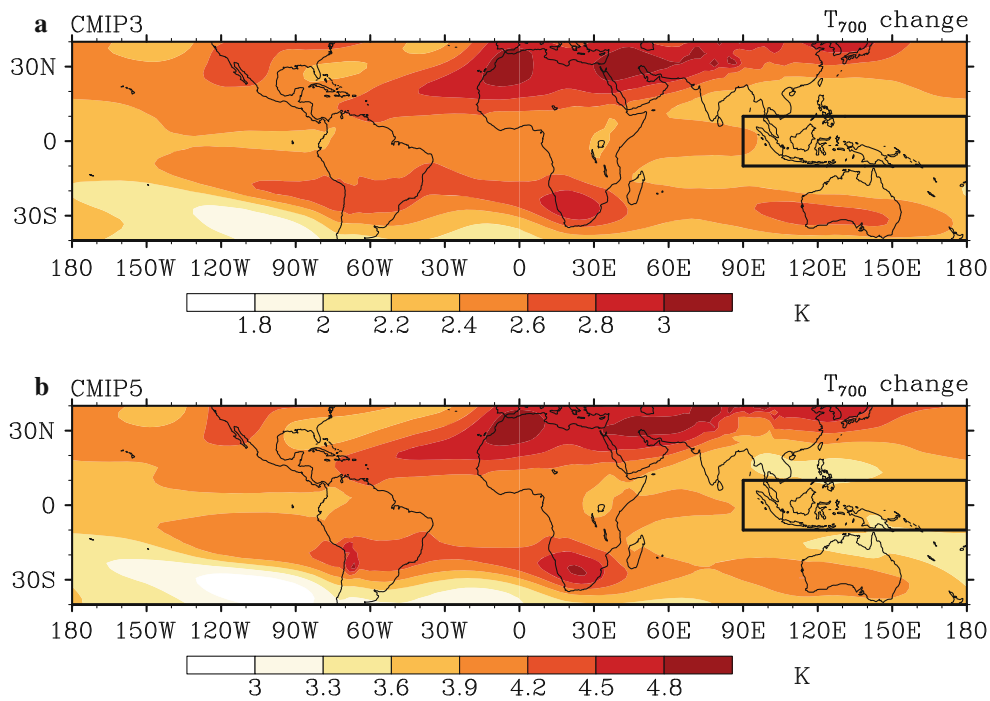


Fig. 5 Geographic distributions of **a** CMIP3 and **b** CMIP5 ensemble-mean T_{700} change. The approximate location of the western Pacific warm pool is represented by the *black box* in each diagram

Percentages of 20th-century interannual LCC variance that can be accounted for by EIS and SST are shown in Fig. 6c, d. Averaged across the regions, the ensemble-mean of the variance accounted for by EIS is 15 % in CMIP3

models and 22 % in CMIP5 models. The ensemble-mean of the variance accounted for by SST is 11 % in both CMIP3 and CMIP5 models. There are large differences in the percentage accounted for across models and regions. In some

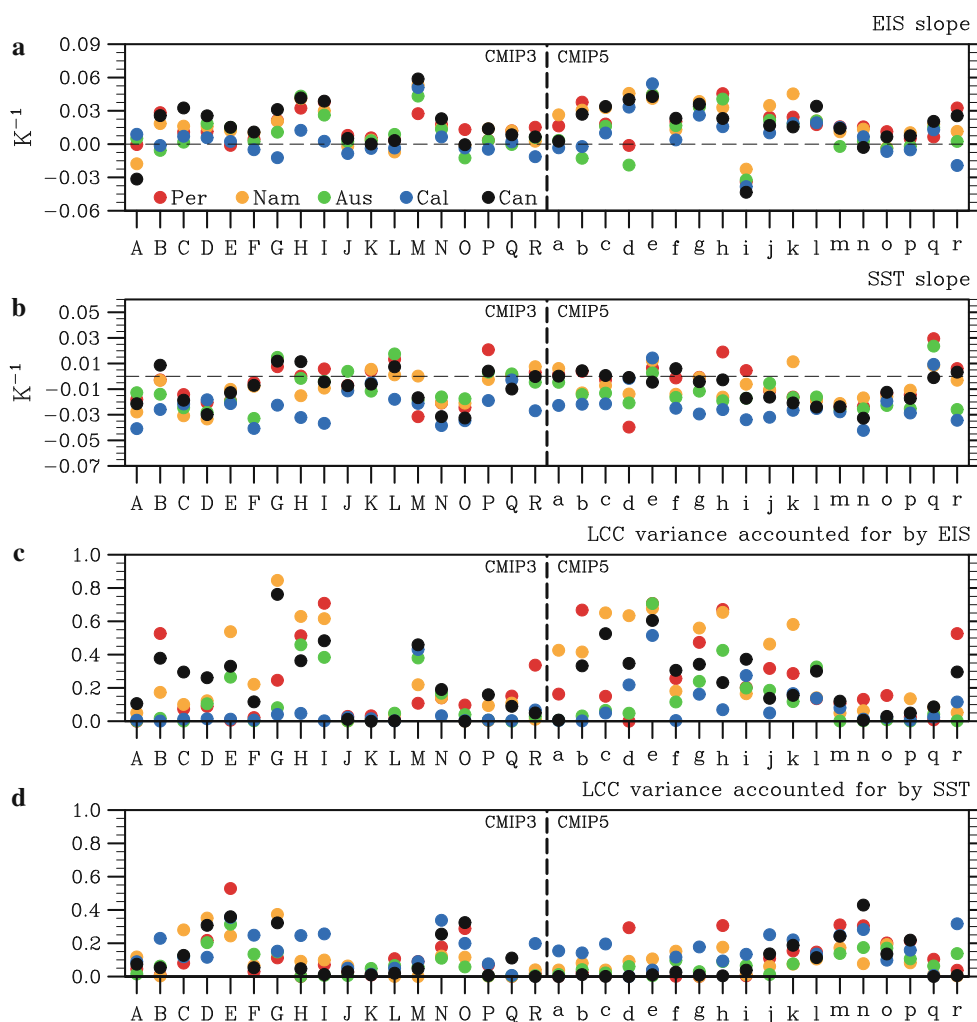


Fig. 6 **a** The EIS slope ($\partial LCC/\partial EIS$), **b** the SST slope ($\partial LCC/\partial SST$) and the percentage of the interannual variance of LCC in the 20th-century that can be accounted for by **c** EIS and **d** SST in the 5 oceanic regions and 36 models

cases, the variables account for relatively little LCC variance, while in others EIS or SST are prime predictors, accounting for up to 60–80 % of the LCC variance. Note that these estimates of EIS and SST contributions to simulated interannual LCC variability understate the roles of EIS and SST somewhat, because they do not include the component of LCC variability that is associated with co-varying EIS and SST anomalies. Of course, variations in atmospheric circulation (e.g., the subsidence rate) or other factors may also be drivers of simulated interannual LCC variability.

5 Contributions to LCC changes

5.1 Roles of various factors

Given anthropogenic changes in EIS and SST and the sensitivities of LCC to changes in EIS and SST calculated from 20th-century variability (i.e., the EIS and SST

slopes), we can quantify the contributions of these environmental changes to simulated LCC changes. For a subset of CMIP5 models, we can use the residual to quantify the respective contributions of GHG, aerosols and environmental parameters other than EIS and SST.

Figure 7a, b show the EIS and SST contributions averaged over the 5 oceanic regions in 36 models. The EIS contribution is generally positive (Fig. 7a) because both the EIS change and the associated slope are generally positive (see Figs. 3a, 6a). In contrast, the SST contribution is negative in almost all the models (Fig. 7b) because the SST change is always positive (see Fig. 3c) and the SST slope is generally negative (see Fig. 6b). Comparison of the two terms reveals that in 27 out of the 36 models (including 14 CMIP3 and 13 CMIP5 models), the magnitude of the SST contribution is larger than that of the EIS contribution. This difference is also reflected in the fact that in both ensembles, the magnitude of the SST contribution is about twice that of the EIS contribution (Table 3).

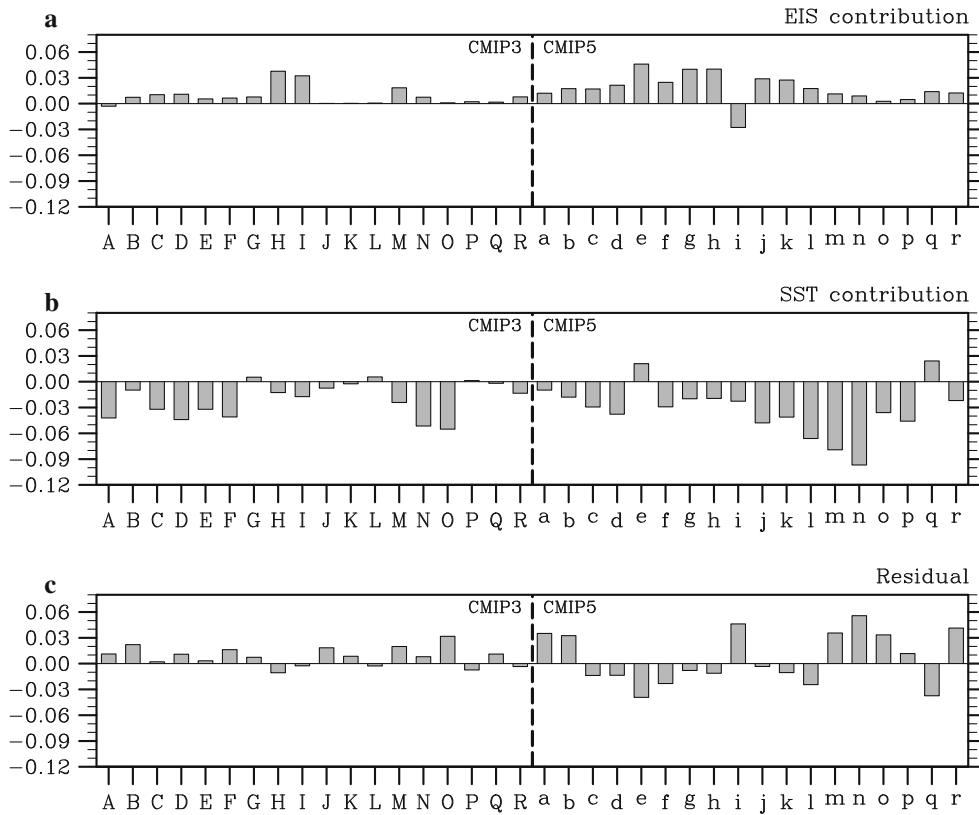


Fig. 7 **a** The EIS contribution to the 21st-century LCC changes averaged over the 5 regions in 36 models. **b** As in (a) but for the SST contribution. **c** As in (a) but for the residual term

Table 3 Various contributions to LCC changes in 36 CMIP models

	CMIP3	CMIP5
EIS	0.86 (1.09)	1.77 (1.66)
SST	-2.08 (2.00)	-3.20 (3.00)
Residual	0.80 (1.11)	0.59 (3.06)

1st row: The ensemble-mean of the EIS contribution averaged over the 5 regions in 18 CMIP3 and 18 CMIP5 models. 2nd row: As in the 1st row, but for the SST contribution. 3rd row: As in the 1st row, but for the residual term. The intermodel standard deviation of all quantities are shown in parentheses. Unit is 0.01

Figure 7c shows the residual term averaged over the 5 oceanic regions in 36 models. While it is generally non-negligible, the residual term is usually not the dominant term. This is demonstrated in Fig. 8, where the magnitude of the residual term is scattered against the maximum of the magnitudes of the EIS and SST contributions. In only 10 out of the 36 models is the residual greater in magnitude than both the EIS and SST contributions. We note that there is no significant anticorrelation across models between the magnitude of the residual term and the portion of 20th-century LCC variance accounted for by EIS and

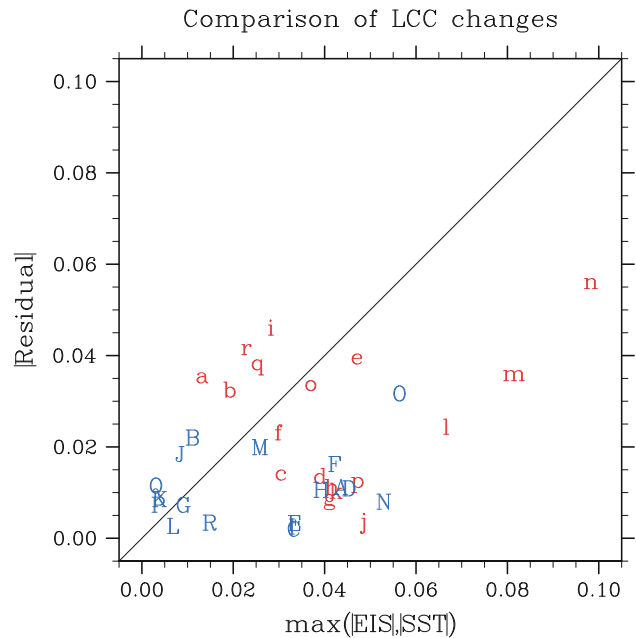


Fig. 8 Scatterplot of the magnitude of the residual term averaged over the 5 oceanic regions versus the maximum of the magnitudes of the EIS and SST contributions averaged over the 5 oceanic regions. CMIP3 models are color-coded in blue, and CMIP5 models in red

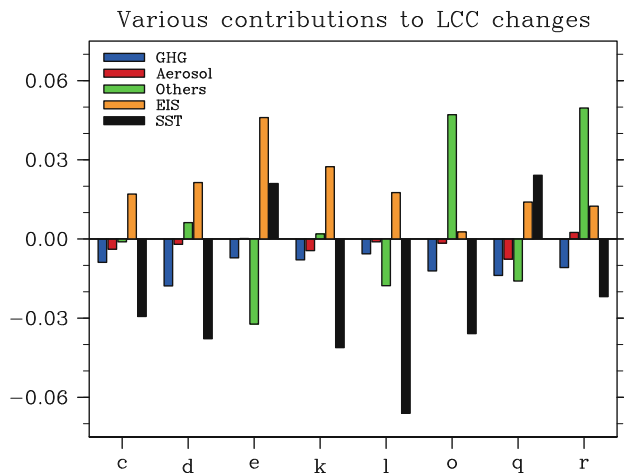


Fig. 9 The respective contributions of GHG (blue bars) and aerosol (red bars) to the residual term averaged over the 5 regions in eight CMIP5 models. The portion of the residual term that is not accounted for by either GHG or aerosol (green bars) is attributed to other factors such as subsidence, horizontal advection and free-tropospheric humidity. For comparison, the respective contributions of EIS and SST to simulated LCC changes are also shown. Note that the indirect effects of aerosol are included in models *c*, *d*, *k*, *l*, *o* and *q*, but not in models *e* and *r*

SST, as one might think. In some of the models with a large residual term (e.g., models B, a, b, i and r), a large fraction of 20th-century LCC variance is actually accounted for by EIS and SST (see Fig. 6).

Figure 9 shows the respective contributions of GHG and aerosol to the residual term in the eight CMIP5 models with data making such an analysis possible. The GHG contribution (blue bars) turns out to be negative in all eight models. Averaged over these models, it is about -0.01 (Table 4). The negative sign of the estimated GHG contribution is consistent with the common view that an increase in GHG concentration decreases low clouds by reducing radiative cooling in the boundary layer (Bretherton et al. 2013). The aerosol contribution (red bars) is also generally negative, consistent with the notion that clouds increase with increasing aerosol concentration. (Recall that aerosols decrease in the RCP8.5 scenario for the 21st century.) However, the magnitude of the aerosol contribution is generally much smaller than that of the GHG contribution (see Table 4). The component of the residual term unrelated to GHG and aerosol, quantified by the difference between the residual term and the overall contributions of GHG and aerosol, is also shown in Fig. 9. It varies a great deal in sign and magnitude from model to model (green bars), and dominates the other components of the residual term (see Table 4). The GHG and aerosol signals in Fig. 9 are consistent across models in the sense that they agree in sign and approximate magnitude. We therefore deem it likely that the GHG and aerosol

Table 4 The respective contributions of GHG, aerosol and environmental factors other than EIS and SST to the regional-mean residual term averaged over eight CMIP5 models

GHG	Aerosol	Others	EIS	SST
-1.05 (0.40)	-0.22 (0.31)	0.47 (2.97)	1.98 (1.28)	-2.34 (3.11)

The respective contributions of EIS and SST to the regional-mean LCC changes averaged over the same eight CMIP5 models are also shown for comparison. The intermodel standard deviation of all quantities are shown in parentheses. Unit is 0.01

contributions are also relatively small components of the residual term in the other CMIP5 models, and in the CMIP3 models. And because the residual term is generally small compared to the EIS and SST contributions, we also conclude that the GHG and aerosol contributions are probably small compared to the EIS and SST contributions in all CMIP3 and CMIP5 models.

5.2 Intermodel spread

Next, we examine the intermodel spread in the various contributions to LCC changes discussed above. Clearly, all three terms on the right side of Eq. (2) contribute to the intermodel spread in LCC changes seen in Fig. 1. To assess their relative importance, we scatter the actual LCC changes against each term in Fig. 10. In both CMIP3 and CMIP5 ensembles, the EIS contribution is only weakly correlated to the actual LCC changes (Fig. 10), suggesting its contribution to LCC spread is relatively small. The SST contribution, in contrast, is significantly correlated with the actual LCC changes. The correlation between the two quantities across CMIP3 models is 0.81, so that about 60 % of the intermodel variance of the actual LCC changes is accounted for by the SST contribution. The correlation across CMIP5 models is 0.69, with 50 % of the intermodel variance of LCC changes being accounted for by the SST contribution. The residual term is weakly correlated or uncorrelated with the actual LCC changes.

Because of the clear dominance of the SST contribution to LCC changes, we look into the relative importance of the SST change and SST slope to the spread in LCC changes. We consider two hypothetical cases: In the first case, in each region, every CMIP3 or CMIP5 model has precisely the same SST change, equal to the respective ensemble-mean SST change averaged over the 5 regions (see Table 2). In this case, the SST contribution in each model is quantified by the product of the SST slope averaged over the 5 regions and the respective ensemble-mean SST change averaged over the 5 regions. Since all CMIP3 or CMIP5 models assume the same SST change, this case is used to isolate the impact of SST slope on the spread in LCC

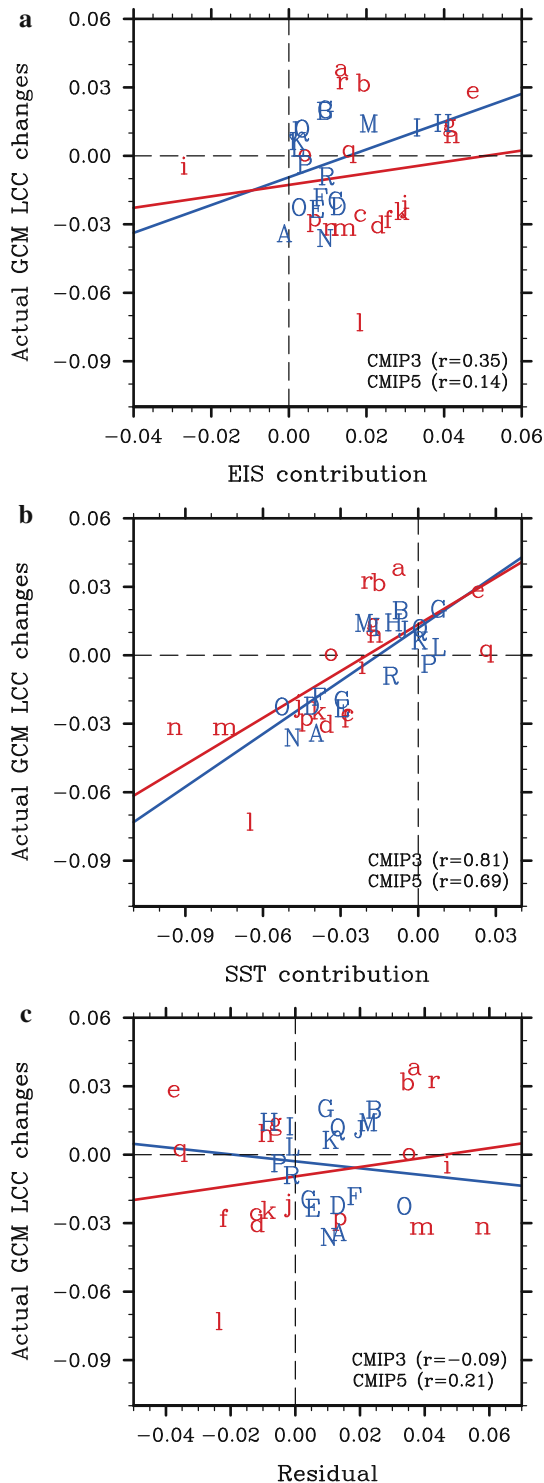


Fig. 10 **a** Scatterplot of the EIS contribution averaged over the 5 regions versus actual LCC changes averaged over the 5 regions. **b** Scatterplot of the SST contribution averaged over the 5 regions versus actual LCC changes averaged over the 5 regions. **c** Scatterplot of the residual term averaged over the 5 regions versus actual LCC changes averaged over the 5 regions. *Solid line* in each diagram represents a least-squares fit regression line. CMIP3 models are color-coded in *blue* and CMIP5 models in *red*

changes. In the second case, in each region, every CMIP3 or CMIP5 model has precisely the same SST slope, equal to the respective ensemble-mean SST slope averaged over the 5 regions (see Table 2). In this case, the SST contribution in each model is quantified by the product of SST change averaged over the 5 regions and the respective ensemble-mean SST slope averaged over the 5 regions. Since all CMIP3 or CMIP5 models assume the same SST slope, this case is used to isolate the impact of the SST change.

We scatter the actual LCC changes against the respective hypothetical SST contributions in both cases described above (Fig. 11). While the SST contribution is well-correlated with the actual LCC changes in both cases, the spread in the SST contribution is much larger in the first case, indicating that the contribution of SST slope to the spread in LCC changes is much larger than the contribution of SST change. Note that the correlation between the SST contribution and the actual LCC changes in the second case may also arise from the feedback of LCC changes on SST: An increase in LCC reduces surface incoming solar radiation, and leads to less surface warming and hence a smaller SST contribution, while a decrease in LCC has the opposite effect.

6 Links to parameterization

6.1 Parameterization and LCC sensitivity to EIS and SST

To assess the impact of parameterizations on simulated LCC changes, we break down PBL and cloud parameterizations used in the 36 models into different types, largely following Moeng and Stevens (2000). We focus on these parameterizations since we expect them to be important for the LCC in these marine stratocumulus regions. Since these parameterizations in the CMIP5 ensemble do not collectively differ in a systematic way from those in the CMIP3 ensemble, we do not distinguish between the two ensembles in the categorization.

In all 36 models, the vertical transport of heat and moisture in PBL is quantified by the product of an eddy diffusivity K and the vertical gradient of heat and moisture. Based on how the eddy diffusivity K is parameterized, we break down the PBL schemes into three categories (see Table 1): (*Category 1*) the “ $K(Ri)$ ” scheme, (*Category 2*) the “ K profile” scheme and (*Category 3*) the “ $K(TKE)$ ” scheme. (See a detailed description of these schemes in “Appendix 3”.) We note that PBL schemes in some models are distinct in that they use cloud-top radiative cooling to drive boundary layer turbulence. These models generally also have an explicit representation of cloud-top entrainment. To examine whether these schemes have any

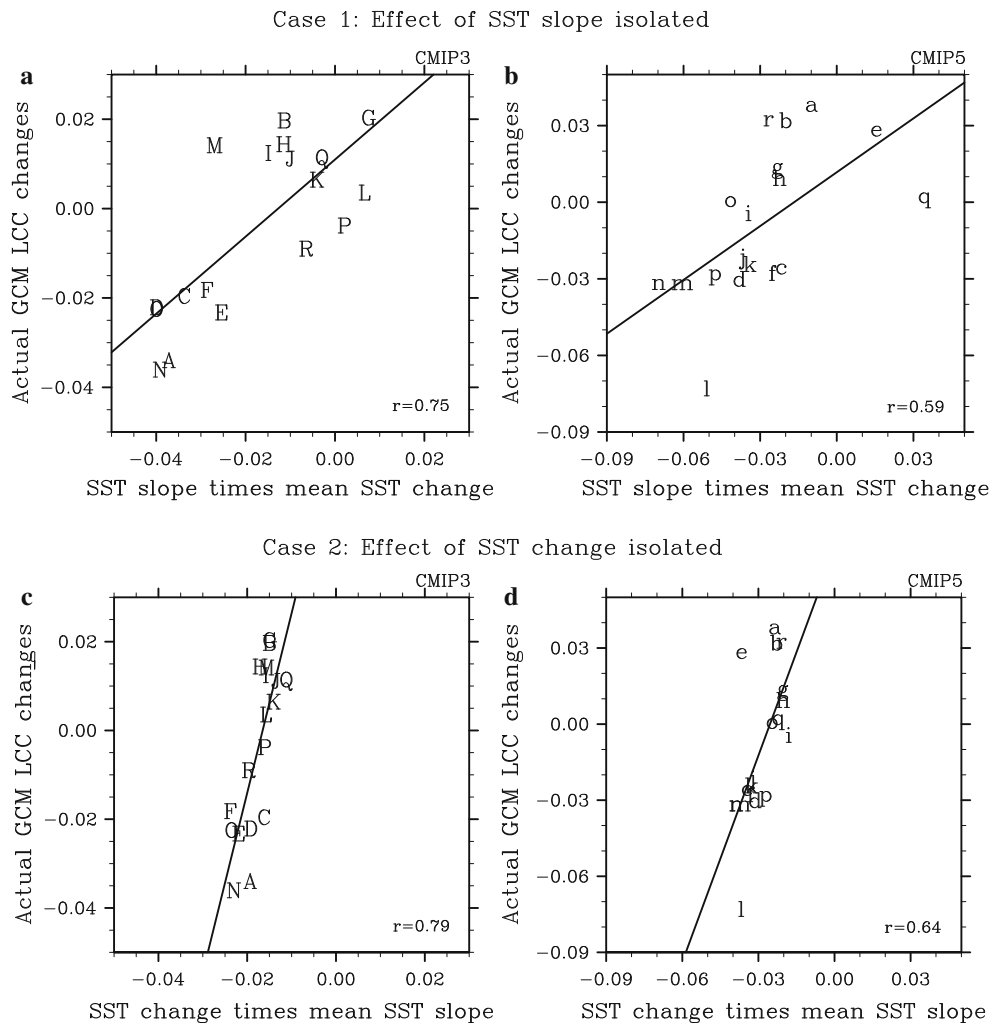


Fig. 11 Scatterplot of actual LCC changes averaged over the 5 regions versus the product of SST slope averaged over the 5 regions and ensemble-mean SST changes averaged over the 5 regions in **a** CMIP3 and **b** CMIP5 models, and scatterplot of actual LCC changes averaged over the 5 regions vs. the product of SST change

averaged over the 5 regions and ensemble-mean SST slope averaged over the 5 regions in **c** CMIP3 and **d** CMIP5. Solid line in each diagram represents a least-squares fit regression line. Note that axes in **a** and **c** have identical scales, and axes in **b** and **d** have identical scales

systematic influences on simulated LCC changes, we analyze these models as a separate category, referred to as the “Top-Driven” scheme.

Depending on whether cloud cover is a prognostic variable, we can break down cloud parameterizations in the 36 models into diagnostic and prognostic schemes. Note that some of the schemes classified below as diagnostic have a prognostic equation for cloud condensate and have been classified in other contexts as prognostic schemes (Jakob 2001; Watanabe et al. 2009). Since our focus is cloud cover rather than cloud condensate, our categorization is entirely based on the models’ treatment of cloud cover.

Based on the key features of the diagnostic schemes, we can further categorize them into three types. This categorization is based on their treatment of stratiform clouds. (In these types of models, convective and stratiform clouds are

usually predicted with separate schemes. We focus on the parameterization of stratiform clouds as the area covered by convective clouds is usually small in these regions.) Thus there are a total of 4 categories of cloud parameterizations, 3 corresponding to diagnostic schemes, and one corresponding to prognostic schemes: (*Category 1*) the “Diag (RH)” scheme, (*Category 2*) the “Diag (RH, stability)” scheme, (*Category 3*) the “Diag (PDF)” scheme and (*Category 4*) the “Prog” scheme. (See a detailed description of these schemes in “Appendix 4”.) Several models in category 2 use the scheme developed by Slingo (1987) or its variant, where marine stratus is parameterized through the observed thermal stability-LCC relationship when the stability of atmospheric column exceeds some threshold value. To further distinguish these models, we refer to them as the “Diag (Slingo)” models. We note that

models tend to use certain combinations of PBL and cloud schemes: Models with the “Diag (PDF)” cloud scheme often use the “ $K(Ri)$ ” PBL scheme, and models with the “Diag (Slingo)” cloud scheme all use the “ K profile” PBL scheme. This characteristics may be attributable to the fact that many CMIP3 and CMIP5 models were developed from a small group of models (See Knutti et al. 2013 for more discussions on this phenomenon).

Given these PBL and cloud parameterizations, we hypothesize how the local sensitivities of LCC to EIS and SST (i.e., the EIS and SST slopes) might emerge in climate simulations. The EIS sensitivity may emerge in two ways. First, in models where thermal stability is used explicitly to parameterize cloud, i.e., those with the “Diag (RH, stability)” cloud scheme, an EIS sensitivity may emerge from the functional dependence of cloud on thermal stability. Second, the EIS sensitivity may emerge indirectly through the models’ dependence of cloud on relative humidity. This is possible because greater thermal stability is often associated with weaker vertical mixing and consequently a shallower and moister PBL. Since all cloud scheme types have at least some relative humidity effect included in their cloud cover formulations, this indirect pathway may occur in every model. A hypothesis borne of the discussions here is that EIS and LCC may be related to one another in all the models, and that the sign and magnitude of the local EIS sensitivity may be influenced by PBL and cloud schemes used in the models and how they interact one another.

The SST sensitivity may emerge primarily through the models’ dependence of cloud on relative humidity. As discussed in the introduction, surface warming increases surface latent heat flux and the moisture contrast between the PBL and free-tropospheric air, leading to a relatively drier and less cloudy PBL when mixing between the PBL and free troposphere occurs. Surface cooling may have the opposite effect on the PBL. The sign and magnitude of the SST slope may also be influenced by PBL and cloud schemes and their interactions in the models because (1) the effect of surface warming on the PBL relative humidity is likely influenced by PBL scheme and (2) the models’ LCC response to relative humidity variations is largely determined by cloud scheme, whether the cloud dependence on relative humidity is implicit or explicit.

It is worth noting that EIS and SST sensitivities may also be influenced by other parameterizations (i.e., shallow convection scheme) or the interactions between parameterizations (Zhang and Bretherton 2008), and thus our categorization is incomplete.

6.2 The role of parameterization

We first assess the impact of parameterization on the sign of LCC changes. Averaged over the 5 regions, the LCC

Table 5 The number of CMIP3 or CMIP5 models where the LCC changes averaged over the 5 oceanic regions are negative (positive), and the breakdown by PBL and cloud scheme type

	CMIP3	CMIP5
Overall	9 (9)	10 (8)
$K(Ri)$	8 (1)	5 (1)
K profile	0 (5)	3 (5)
$K(TKE)$	1 (3)	2 (2)
Top-driven	0 (2)	3 (2)
Diag (RH)	1 (1)	1 (0)
Diag (RH, stability)	2 (6)	2 (4)
Diag (Slingo)	0 (3)	0 (4)
Diag (PDF)	6 (0)	6 (2)
Prog	0 (2)	1 (2)

changes are predominantly negative in models with the “ $K(Ri)$ ” PBL scheme and the “Diag (PDF)” cloud scheme, while they are positive in models with the “Diag (Slingo)” cloud scheme (Table 5). Note that while the averaged LCC changes are also generally positive in models with the “ K profile” PBL scheme and the “Diag (RH, stability)” cloud scheme, this sign preference is found to originate largely from models with the “Diag (Slingo)” cloud scheme. The influence of other scheme types such as the “ K (TKE)” and “Top-Driven” PBL schemes and the “Diag (RH)” and “Prog” cloud schemes is less clear. We note that these schemes are used only in a small subset of the 36 models, so it is difficult to robustly assess their influence on the sign of LCC changes.

Next, we assess the impact of parameterization on the magnitude of LCC changes. Figure 12 shows LCC changes averaged over the 5 oceanic regions in the 36 models, color-coded by PBL and cloud schemes used in the models. We find that parameterization plays a significant role in determining the magnitude of LCC changes: Models with a large LCC decrease are mostly those with the “ $K(Ri)$ ” PBL scheme and “Diag (PDF)” cloud scheme, while models with a large LCC increase are mostly those with the “Diag (Slingo)” cloud scheme. The variety of scheme types therefore may contribute significantly to the intermodel spread in the average LCC changes. Note that the magnitude of the average LCC changes also varies considerably within each of these PBL or cloud scheme types. Differences in the implementation of these schemes in the models may be partly responsible for the variations with the same scheme type. In some cases, intermodel differences in the anthropogenic changes in the large-scale atmospheric environment may also play a role.

As demonstrated in Sect. 5, the SST slope is clearly a significant factor in determining the size of the SST contribution, and is therefore also a significant determinant of

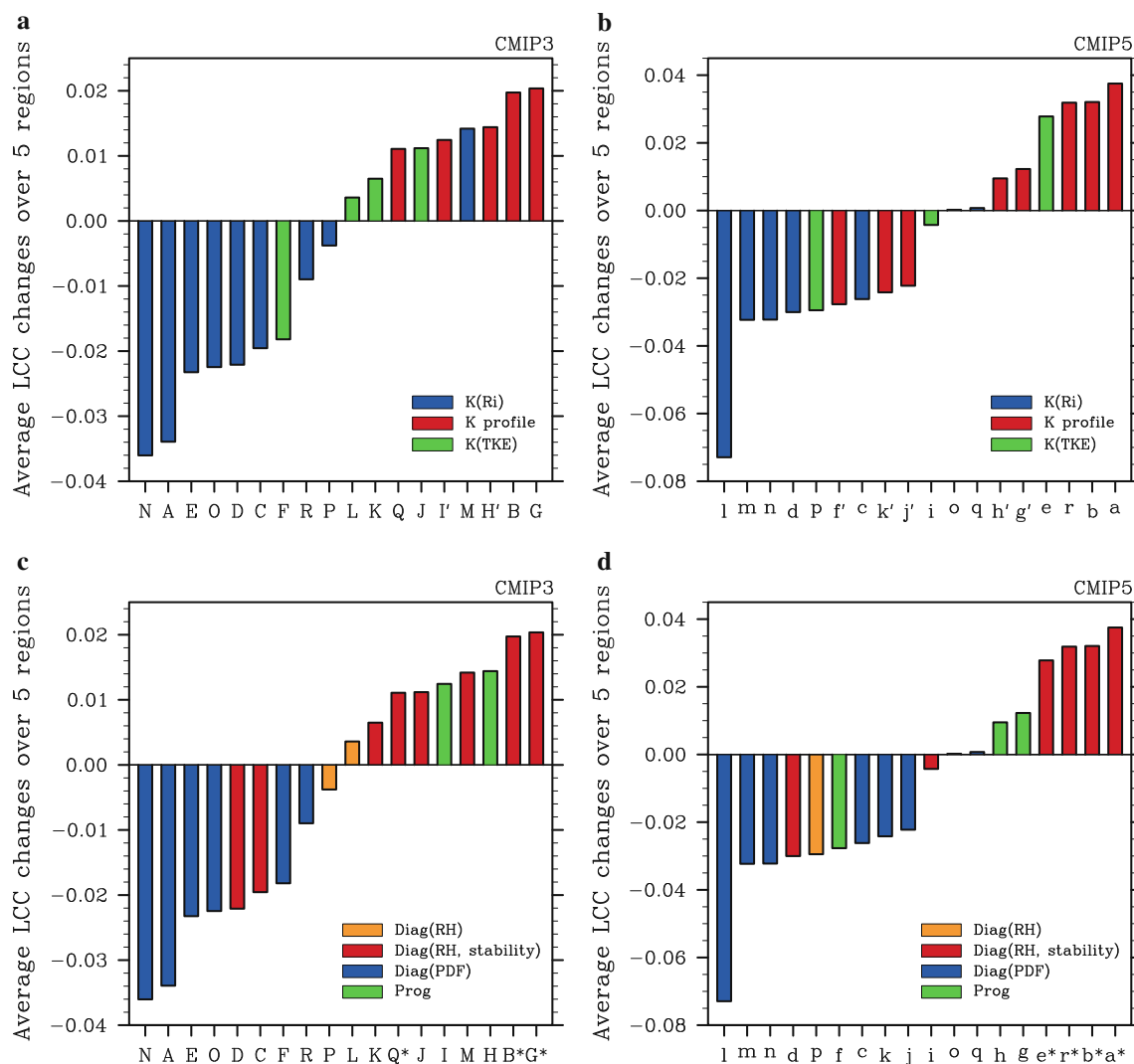


Fig. 12 The LCC changes averaged over the 5 oceanic regions in 36 models, organized in ascending order and color-coded by PBL scheme type in (a) and (b), and cloud scheme type in (c) and (d). CMIP3 models are shown in (a) and (c), and CMIP5 models in

(b) and (d). Models with the “Top-Driven” PBL scheme are identified by a prime following their reference letters, and models with the “Diag (Slingo)” cloud scheme by an *asterisk* following their reference letters

the sign and magnitude of the LCC changes. We focus on it here to understand better the association between PBL and cloud scheme types and LCC changes demonstrated above. Figure 13 shows the SST slope averaged over the 5 oceanic regions in the 36 models, color-coded by PBL and cloud schemes used in the models. Models with a large negative SST slope are mostly those with the “ $K(Ri)$ ” PBL scheme and “Diag (PDF)” cloud scheme. This may explain why simulated LCC changes are consistently negative in models with these schemes. Likewise, we find that models with a small or even positive SST slope are mostly those with the “Diag (Slingo)” cloud scheme. This may explain why simulated LCC changes are consistently positive in models with this scheme. For completeness, we also examine the association between the EIS slope and parameterization

(Fig. 14). However, we do not find any systematic relationship between them. Interestingly, even in models where stability is explicitly used in the cloud scheme (i.e., the “Diag (RH, stability)” and “Diag (Slingo)” schemes), the EIS slope is not systematically greater than the slope in other models.

7 Comparison with observation

Estimates of observed EIS and SST slopes in the 5 oceanic regions are shown in Table 6. The observed EIS slope is positive in all regions except the Californian region. Averaged over all regions, the observed EIS slope is about 0.026 K^{-1} . This is less than half the EIS slope derived from

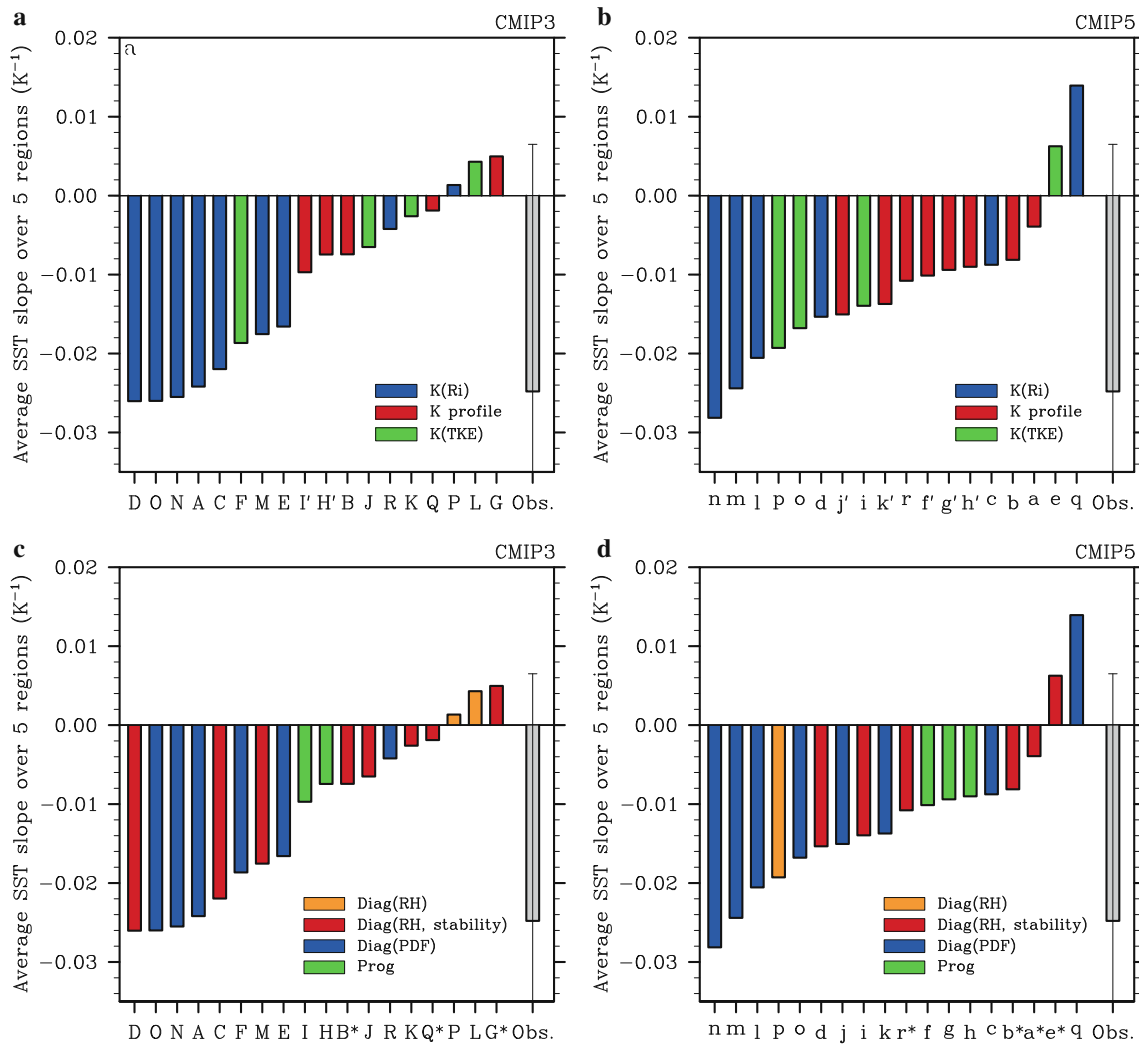


Fig. 13 SST slope averaged over the 5 oceanic regions in 36 models, organized in ascending order and color-coded by PBL scheme type in (a) and (b), and cloud scheme type in (c) and (d). CMIP3 models are shown in (a) and (c), and CMIP5 models in (b) and (d). Models with the “Top-Driven” PBL scheme are identified by a prime following

their reference letters, and models with the “Diag (Slingo)” cloud scheme by an *asterisk* following their reference letters. For comparison, the observed SST slope (*gray bars*) and its confidence interval (*gray lines*) are also shown. Note that the lower bound of the confidence interval is out of the range of *y-axis*

interregional and seasonal covariability of LCC and EIS ($\sim 0.06 \text{ K}^{-1}$, Wood and Bretherton 2006). The difference stems in part from methodology. In this study, the influence of SST on LCC and EIS variations was removed before calculating the EIS slope, while it was included in Wood and Bretherton (2006). If the methodology in Wood and Bretherton (2006) were adopted in our analysis, the observed EIS slope averaged over all regions would rise to approximately 0.04 K^{-1} . Sources of the remaining difference may include (1) differences in the definition of LCC, (2) differences in cloud data used, and (3) statistical uncertainty in deriving the slope.

We find that the observed SST slope is negative in all regions, with an average of about -0.025 K^{-1} over all regions. Based on monthly gridded data, from the Clouds and

the Earth’s Radiant Energy System (CERES)—*Terra*, a recent estimate of the SST slope gives a range of -0.019 to -0.034 K^{-1} (Eitzen et al. 2011). Though our average value is within this range, the Eitzen et al. estimate was derived without removing the influence of EIS on LCC and SST variations. When we estimate the SST slope without excluding this influence, the result is close to -0.04 K^{-1} , slightly greater than the upper bound of the estimate in Eitzen et al. (2011), but still in approximate agreement. As with the EIS slope, sources of the difference between Eitzen et al. (2011) and this study may include (1) differences in the definition of LCC, (2) differences in cloud data used, and (3) statistical uncertainty in deriving the slope. Note also that the confidence intervals in Table 6 are large, partly because of the relatively short temporal coverage of ISCCP cloud data.

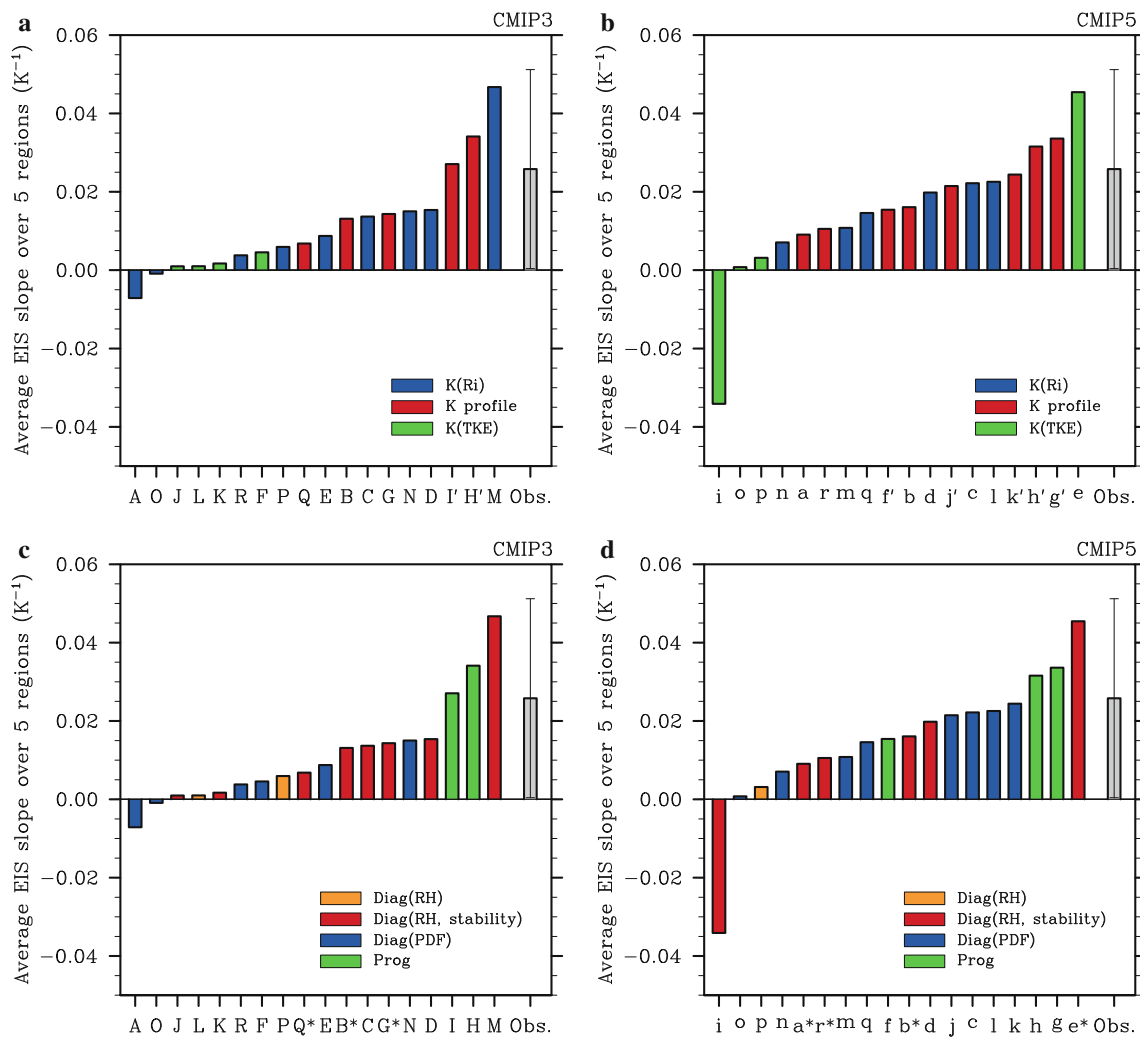


Fig. 14 EIS slope averaged over the 5 oceanic regions in 36 models, organized in ascending order and color-coded by PBL scheme type in (a) and (b), and cloud scheme type in (c) and (d). CMIP3 models are shown in (a) and (c), and CMIP5 models in (b) and (d). Models with the “Top-Driven” PBL scheme are identified by a prime following

their reference letters, and models with the “Diag (Slingo)” cloud scheme by an *asterisk* following their reference letters. For comparison, the observed EIS slope (gray bars) and its confidence interval (gray lines) are also shown

Table 6 Estimates of observed EIS and SST slopes as well as the 95% confidence intervals of these estimates in the 5 oceanic regions

	Per	Nam	Aus	Cal	Can	Overall
EIS slope	5.54 (±1.84)	3.49 (±2.07)	3.85 (±2.08)	-2.07 (±3.94)	2.07 (±2.78)	2.58 (±2.54)
SST slope	-0.39 (±2.09)	-2.42 (±3.04)	-1.16 (±2.44)	-6.81 (±5.39)	-1.63 (±2.72)	-2.48 (±3.13)
R ² (LCC, EIS)	0.61	0.33	0.38	0.05	0.09	0.29
R ² (LCC, SST)	0.01	0.10	0.04	0.22	0.06	0.08

To obtain observed EIS and SST slopes, in each region we first compute annual-mean and regional-mean LCC time series based on ISCCP cloud data, annual-mean and regional-mean EIS time series based on ERA-Interim reanalysis and annual-mean and regional-mean SST time series based on NOAA optimum interpolation monthly SST version 2 (see also Sect. 2). Then we remove the long-term trend from each of the LCC, EIS and SST time series and perform regression analyses described in “Appendix 1”. Based on these analyses, we also compute the 95 % confidence intervals of the slope estimates. The percentages of the interannual variance of LCC that can be accounted for by EIS and SST are also shown for each of the 5 oceanic regions, as well as the respective averages of the slopes, confidence intervals and the percentages accounted for by EIS and SST over the 5 oceanic regions. Unit for the estimated slopes is 0.01 K⁻¹

Percentages of observed interannual LCC variance that can be accounted for by EIS and SST are also shown in Table 6 for each of the 5 oceanic regions. Averaged over all the regions, the percentage of the LCC variance accounted for by EIS is 0.29, while the percentage of the LCC variance accounted for by SST is 0.08. The only exception to this is in the Californian region, where the percentage of the LCC variance accounted for by SST is about 4 times that accounted for by EIS. (A similar difference in the relative magnitudes of LCC-SST and LCC-LTS correlations in this region is also reported in Clement et al. (2009).)

Finally, we use estimates of observed SST and EIS slopes to assess the realism of simulated SST and EIS slopes. Simulated slopes generally have signs consistent with the observed slopes—negative for SST slope and positive for EIS slope (Figs. 13, 14). And in many models, the simulated slopes agree well with their observed counterparts. The qualitative similarity between the models as an ensemble and the observations supports the idea that the models generally capture the real LCC sensitivity to key environmental conditions. Nevertheless, models generally underestimate the magnitudes of both SST and EIS slopes. Models with the largest underestimation of SST slope or even a positive SST slope are primarily those with the “Diag (Slingo)” cloud scheme. (These models generally exhibit a large LCC increase (see Fig. 12).) In contrast, models with realistic SST slope (including models A, D, N, O, m and n) are primarily those with the “ $K(Ri)$ ” PBL scheme and “Diag (PDF)” cloud scheme. (These models generally exhibit a large LCC decrease (see Fig. 12).) Unlike the SST slope, the underestimation of EIS slope is not associated with particular parameterization schemes. This is consistent with the fact that there is no systematic relationship between the EIS slope and parameterization (see Sect. 6). Note that the underestimation of EIS slope is generally greater in the CMIP3 ensemble than CMIP5 (Fig. 14). With regard to the percentages of the LCC variance accounted for by EIS and SST, both CMIP3 and CMIP5 ensembles underestimate the percentage accounted for by EIS somewhat (0.15 and 0.22 vs. 0.29), but slightly overestimate the percentage accounted for by SST (0.11 vs. 0.08, Table 6 and Sect. 4). This general qualitative agreement between the models and observations again supports the idea that the models as an ensemble have roughly the right EIS and SST sensitivities and the right balance between variability due to these factors and other environmental factors.

So what do these observational estimates imply about future LCC change? Focusing on the competition between EIS and SST effects, we have seen that the observed EIS and SST slopes are comparable in magnitude, as are those of the models. This leaves the relative magnitudes of the

future EIS and SST changes to determine which effect wins. The models predict the SST increase will be much larger than the increase in EIS (Table 2; Fig. 3). This is also physically reasonable. For the EIS change to be larger than the SST change, the surface and 700 hPa warming would have to be completely decoupled from one another in the LCC regions, a very unlikely outcome. In reality and in the models, large-scale dynamics will constrain the surface and 700 hPa warming so that to zero order, the vertical atmospheric temperature structure remains close to a moist adiabat, with the EIS change then representing the relatively subtle departure from that situation. Based on these arguments, we conclude that the larger simulated magnitude of the SST change is physical, and that the negative contribution of SST to LCC changes would outweigh the positive contribution of EIS, reducing LCC. Thus if EIS and SST effects alone are considered, it is likely LCC would decrease over the 21st-century. However, the residual term representing other effects is not negligible in many models (Fig. 7), so we cannot exclude the outcome where the LCC change occurs for reasons other than an EIS or SST change. There are also large statistical uncertainties in our estimates of observed SST and EIS slopes (Table 6). For these reasons, we have only medium overall confidence that LCC will decrease.

8 Summary and discussions

In this study, we quantify the linear contributions of EIS and SST to LCC changes in 36 climate change simulations associated with phases 3 and 5 of the Coupled Model Intercomparison Project. LCC changes not attributable to either EIS or SST changes (the residual term) are attributed to changes in GHG and aerosol concentrations, environmental factors other than EIS and SST, and the nonlinear effects of EIS and SST. Among the three terms in the heuristic model (the EIS and SST contributions and the residual term), the SST term emerges as the dominant source of the intermodel spread in LCC changes. It accounts for nearly two-thirds of the intermodel variance of LCC changes in CMIP3 models and about half of it in CMIP5 models. These results validate the central assumptions of the heuristic model: The anthropogenic LCC changes can be mostly understood through a small number of large-scale controls (one is enough, as it turns out!), and the sensitivities in the context of climate change can be potentially diagnosed from interannual variability.

The global models’ sensitivity to changes in SST varies a great deal from model to model, driving a large part of the intermodel spread in LCC changes. (The large intermodel spread in the sensitivity of marine low clouds to SST is also demonstrated in Bony and Dufresne (2005).) LCC

generally increases in models with a small SST sensitivity, while it decreases in models with a large SST sensitivity. This sensitivity is strongly influenced by cloud and boundary layer parameterization in the global models. The “ $K(Ri)$ ” PBL scheme, in which the PBL eddy diffusivity K is related in simple ways to the local Richardson number, and the “Diag (PDF)” cloud scheme, in which cloud cover is determined by accounting for the sub-grid scale variability of moisture and temperature, favor a large SST sensitivity, and a large decrease in LCC. In contrast, the “Diag (Slingo)” scheme, in which low clouds are parameterized primarily through the observed thermal stability-LCC relationship, favors a small SST sensitivity. Models with this scheme exhibit a large increase in LCC.

Comparison with the estimate of observed SST sensitivity reveals that models with the “ $K(Ri)$ ” PBL scheme and “Diag (PDF)” cloud scheme generally simulate a realistic SST sensitivity, while models with the “Diag (Slingo)” cloud scheme underestimate it. The underestimation of SST sensitivity is somewhat expected in the “Diag (Slingo)” scheme because under some conditions, cloud cover is diagnosed with thermal stability in this scheme. When these conditions are met, cloud cover has no sensitivity to SST variations that are independent of variations in thermal stability. This leads to a vanishingly small value of SST sensitivity. Most models underestimate the observed EIS sensitivity. (The underestimation of EIS sensitivity in the CMIP3 ensemble was also found in Caldwell et al. (2013).) While this systematic bias may contribute little to the intermodel spread in LCC changes, it has the effect of moving the spectrum of simulated LCC changes towards negative values.

The respective contributions of GHG and aerosol in a subset of CMIP5 models with available data are also quantified in this work. The GHG contribution is modest, and consistently negative in these models, supporting the view that an increase in GHG concentration decreases simulated low clouds by reducing radiative cooling in the boundary layer. The aerosol contribution is also mostly negative, but its magnitude is even smaller than that of the GHG contribution. The intermodel spread in either the GHG or aerosol contribution turns out to be much smaller than the intermodel spread in the LCC changes that cannot be unambiguously linked to SST or EIS changes (residual term). This indicates that meteorological factors such as subsidence, horizontal advection, free-tropospheric moisture, or nonlinear effects of LCC and EIS changes are the main remaining sources of spread in the residual term.

In spite of all the potential complexity underlying anthropogenic changes in LCC, the heuristic model predicts LCC will decrease over the 21st-century. This assessment is based on two facts: (1) The observed EIS and

SST slopes are comparable in magnitude, and (2) the future SST increase ought to be larger than the future EIS increase. (This is a common feature of the models and one that makes sense physically.) However, the residual term representing other effects is not negligible in many models, so we cannot exclude the outcome where the LCC change occurs for reasons other than an EIS or SST change. There are also large statistical uncertainties in our estimates of observed SST and EIS slopes. For these reasons, we have only medium overall confidence that LCC will decrease. Longer observational records and a careful assessment of other environmental factors producing LCC changes are needed to place a stronger constraint on simulated LCC changes. Meanwhile, addressing biases in simulated SST and EIS sensitivities will clearly be an important step towards reducing uncertainties in this aspect of climate change.

Acknowledgments All authors are supported by DOE’s Regional and Global Climate Modeling Program under the project “Identifying Robust Cloud Feedbacks in Observations and Model” (contract DE-AC52-07NA27344). The work of LLNL authors was performed under the auspices of the United States Department of Energy by Lawrence Livermore National Laboratory under contract DE-AC52-07NA27344. We acknowledge the modeling groups, the Program for Climate Model Diagnosis and Intercomparison (PCMDI) and the WCRP’s Working Group on Coupled Modelling (WGCM) for their roles in making available the WCRP CMIP3 and CMIP5 multi-model datasets. Support of these datasets is provided by the Office of Science, U.S. Department of Energy. We thank Drs. Yunyan Zhang, Mark Zelinka, Florent Briant, Fengpeng Sun and Heng Xiao for many stimulating discussions on the topic and Alexandre Jousse for his help with MODIS data set. We also thank two anonymous reviewers for their constructive comments on the original manuscript. ISCCP cloud data is downloaded from <http://www.cgd.ucar.edu/>, ERA-Interim data from <http://www.ecmwf.int/>, NOAA optimum interpolation monthly SST version 2 from <http://www.esrl.noaa.gov/>.

Appendix 1: Calculating EIS and SST slopes

EIS slope is calculated based on detrended time series of LCC, EIS and SST in 20th-century (LCC' , EIS' , SST') as follows. First, we regress EIS' onto SST' ($EIS' \approx \alpha_1 \cdot SST' + \alpha_0$). Then we tease out the component of EIS' uncorrelated with SST' , EIS'_{clean} ($= EIS' - \alpha_1 \cdot SST'$). Third, we regress LCC' onto SST' ($LCC' \approx \beta_1 \cdot SST' + \beta_0$), and tease out the component of LCC' uncorrelated with SST' , LCC'_{clean} ($= LCC' - \beta_1 \cdot SST'$). Finally, we regress LCC'_{clean} onto EIS'_{clean} ($LCC'_{clean} \approx \gamma_1 \cdot EIS'_{clean} + \gamma_0$). EIS slope assumes the value of γ_1 .

Likewise, to calculate SST slope, we first regress SST' onto EIS' ($SST' \approx \alpha_1 \cdot EIS' + \alpha_0$). Then we tease out the component of SST' uncorrelated with EIS' , $SST'_{clean} = (SST' - \alpha_1 \cdot EIS')$. Third, we regress LCC' onto EIS' ($LCC' \approx \beta_1 \cdot EIS' + \beta_0$), and tease out the component of LCC' uncorrelated with EIS' , $LCC'_{clean} =$

$(LCC' - \beta_1 \cdot EIS')$. Finally, we regress LCC'_{clean} onto SST'_{clean} ($LCC'_{clean} \approx \gamma_1 \cdot SST'_{clean} + \gamma_0$). SST slope assumes the value of γ_1 .

Using the methodology described above, we also estimate EIS and SST slopes in pre-industrial control simulations and 21st-century simulations (scenario A1B for CMIP3 models and RCP 8.5 for CMIP5 models) with 18 CMIP3 and 18 CMIP5 models (The long-term trends in LCC, EIS and SST in the 21st-century simulations were removed before calculating EIS and SST slopes.). Figure 15a scatters the EIS slope in the historical simulations against the EIS slope in their corresponding pre-industrial control simulations, and Fig. 15b scatters the EIS slope in the historical simulations against the EIS slope in their corresponding 21st-century simulations. The EIS slope exhibits a high degree of correspondence among different simulations of each CMIP3 or CMIP5 model. Figure 15c scatters the SST slope in the historical simulations against the SST slope in their corresponding pre-industrial control

simulations, and Fig. 15d scatters the SST slope in the historical simulations against the SST slope in their corresponding 21st-century simulations. The SST slope also exhibits a high degree of correspondence among different simulations of each CMIP3 or CMIP5 model, though some discrepancy in this quantity between the historical and 21st-century simulations is visible.

Appendix 2: An analytical expression for EIS change

Based on the definition of LTS, we rewrite Eq. (1) as follows

$$EIS = T_{700} \cdot \left(\frac{1000}{700}\right)^{Ra/c_p} - T_s \cdot \left(\frac{1000}{p_s}\right)^{Ra/c_p} - \Gamma_m^{850} \cdot (z_{700} - LCL) \tag{4}$$

where Ra ($=287 \text{ J K}^{-1} \text{ kg}^{-1}$) is gas constant for air, c_p ($=1,004 \text{ J K}^{-1} \text{ kg}^{-1}$) is specific heat of air at constant

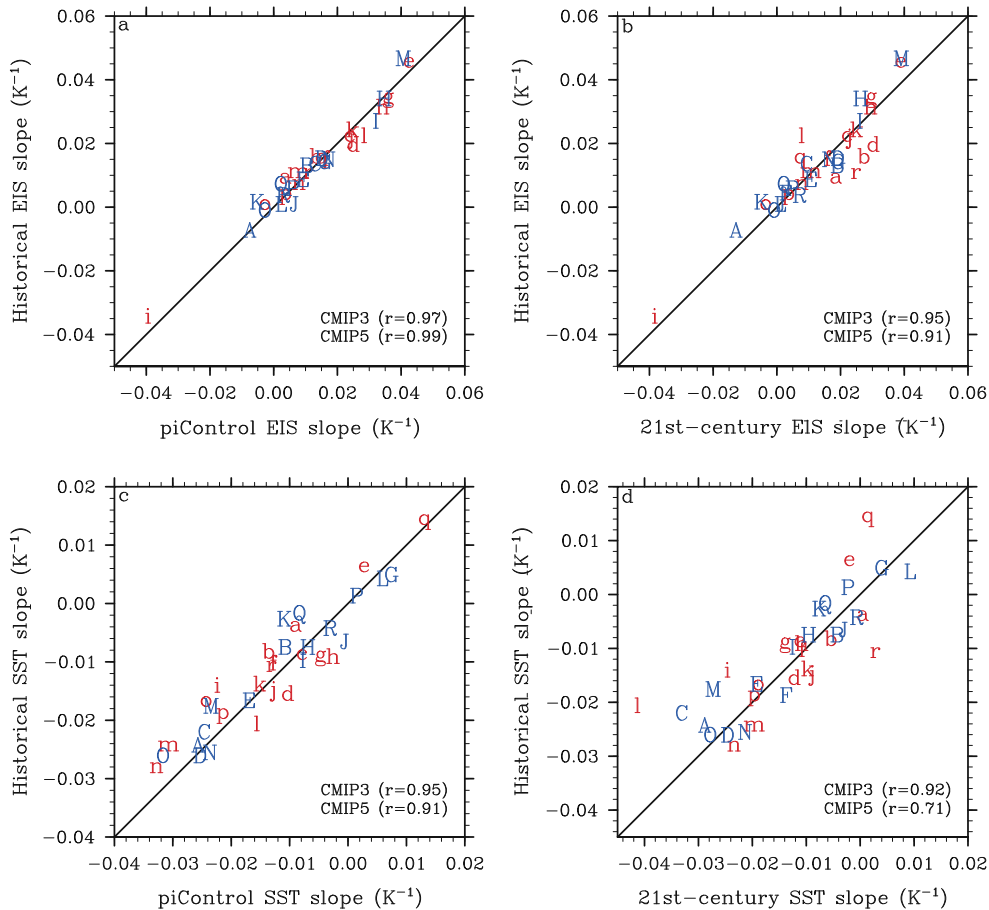


Fig. 15 **a** Scatterplot of the EIS slope in the historical simulations versus the EIS slope in the respective pre-industrial control simulations in 36 models. **b** Scatterplot of the EIS slope in the historical simulations versus the EIS slope in the respective 21st-century simulations in 36 models. **c** As in (a) but for the SST slope. **d** As in (b) but for the SST slope. In each model, the EIS or SST slope is first

calculated for each region and then averaged over the 5 regions. CMIP3 models are color-coded in blue and CMIP5 models in red. Solid line in each diagram represents the line $y = x$. Note that the pre-industrial control simulation with model F has no cloud data, so it is not shown in panels (a) and (c)

pressure, and p_s is surface pressure, typically, 1,020 hPa. Treating z_{700} and LCL as constants, we obtain an expression for EIS change

$$\Delta EIS = 1.11 \cdot \Delta T_{700} - 0.99 \cdot \Delta T_s - \frac{d\Gamma_m^{850}}{dT_{850}} \cdot \Delta T_{850} \cdot (z_{700} - LCL) \quad (5)$$

Consistent with Wood and Bretherton (2006), we approximate T_{850} by the mean of T_s and T_{700} . So, $\Delta T_{850} = \frac{1}{2} \cdot (\Delta T_s + \Delta T_{700})$. Based on the formula for Γ_m^{850} in Wood and Bretherton (2006) and assuming some typical values for T_s , T_{700} and surface relative humidity (respectively: 295, 280 K and 80 %), we obtain $d\Gamma_m^{850}/dT_{850} = 1 \times 10^{-4} \text{ m}^{-1}$, $z_{700} = 3250 \text{ m}$ and $LCL = 430 \text{ m}$. With these estimates, we arrive at an analytical expression for EIS change.

$$\Delta EIS \approx 0.97 \cdot \Delta T_{700} - 1.14 \cdot \Delta T_s \quad (6)$$

Appendix 3: PBL parameterization

The three categories of PBL schemes are described in order of increasing complexity:

Category 1, the “K(Ri)” scheme. In 15 of the 36 models (models A, C, D, E, M, N, O, P, R, c, d, l, m, n and q), K is parameterized as a decreasing function of the local Richardson number Ri , with unstable situations ($Ri < 0$) associated with a larger K than stable situations ($Ri > 0$).

Category 2, the “K profile” scheme. In 13 of the 36 models (models B, G, H, I, Q, a, b, f, g, h, j, k and r), a fixed vertical profile of K is assumed when boundary layers are unstable ($Ri < 0$): K peaks somewhere inside the PBL and decreases towards both the surface and PBL top where it vanishes. When boundary layers are stable ($Ri > 0$), the K is parameterized as a decreasing function of Ri as in the “ $K(Ri)$ ” scheme.

Category 3, the “K(TKE)” scheme. In 8 of the 36 models (models F, J, K, L, e, i, o and p), K is parameterized as a function of turbulent kinetic energy (TKE). TKE is predicted with a prognostic equation including terms corresponding to generation by wind shear and buoyancy, a vertical transport term, and a dissipation term.

Appendix 4: Cloud cover parameterization

The four categories of cloud schemes are described in order of increasing complexity:

Category 1, the “Diag (RH)” scheme. In 3 of the 31 diagnostic models (models L, P and p), cloud cover is a simple function of relative humidity.

Category 2, the “Diag (RH, stability)” scheme. In 14 of the remaining diagnostic models (models B, C, D, G, J, K,

M, Q, a, b, d, e, i and r), cloud cover is parameterized through relative humidity with some consideration of thermal stability effects.

Category 3, the “Diag (PDF)” scheme. In the final 14 of the diagnostic models (models A, E, F, N, O, R, c, j, k, l, m, n, o and q), cloud cover is determined by accounting for the sub-grid scale variability in both total water content and temperature. This variability often assumes some simple probability density functions (PDFs).

Category 4, the “Prog” scheme. A prognostic scheme developed by Tiedtke (1993) is implemented in five models (models H, I, f, g and h). In this scheme, cloud cover is determined by a prognostic equation that accounts for various cloud formation and dissipation processes.

References

- Albrecht BA (1989) Aerosols, cloud microphysics, and fractional cloudiness. *Science* 245:1227–1230
- Andrews T, Gregory JM, Webb MJ, Taylor KE (2012) Forcing, feedbacks and climate sensitivity in CMIP5 coupled atmosphere-ocean climate models. *Geophys Res Lett* 39:L09712. doi:10.1029/2012GL051607
- Bao Q et al (2013) The flexible global ocean-atmosphere-land system model, spectral version 2: FGOALS-s2. *Adv Atm Sci* 30:561–576. doi:10.1007/s00376-012-2113-9
- Bentsen M et al (2012) The Norwegian earth system model, NorESM1-M—part 1: description and basic evaluation. *Geosci Model Dev Discuss* 5:2843–2931
- Bony S et al (2006) How well do we understand and evaluate climate change feedback processes? *J Clim* 19:3445–3482
- Bony S, Dufresne JL (2005) Marine boundary layer clouds at the heart of tropical cloud feedback uncertainties in climate models. *Geophys Res Lett* 32:L20806. doi:10.1029/2005GL023851
- Bretherton CS, Wyant MC (1997) Moisture transport, lower tropospheric stability and decoupling of cloud-topped boundary layers. *J Atmos Sci* 54:148–167
- Bretherton CS, Blossey PN, Jones CR (2013) Mechanisms of marine low cloud sensitivity to idealized climate perturbations: a single-LES exploration extending the CGILS cases. *J Adv Model Earth Syst* 5. doi:10.1002/jame.20019
- Brient F, Bony S (2012) Interpretation of the positive low cloud feedback predicted by a climate model under global warming. *Clim Dyn*. doi:10.1007/s00382-011-1279-7
- Caldwell PM, Zhang Y, Klein SA (2013) CMIP3 subtropical stratocumulus cloud feedback interpreted through a Mixed-Layer Model. *J Clim* 26:1607–1625
- Cess RD et al (1990) Intercomparison and interpretation of climate feedback processes in 19 atmospheric general circulation models. *J Geophys Res* 95:16601–16615
- Chen J, Rossow WB, Zhang Y (2000) Radiative effects of cloud-type variations. *J Clim* 13:264–286
- Chung D, Teixeira J (2012) A simple model for stratocumulus to shallow cumulus cloud transitions. *J Clim* 25:2547–2554. doi:10.1175/JCLI-D-11-00105.1
- Chylek P, Li J, Dubey MK, Wang M, Lesins G (2011) Observed and model simulated 20th century Arctic temperature variability: Canadian Earth System Model CanESM2. *Atmos Chem Phys Discuss* 11:22893–22907. <http://www.atmos-chem-phys-discuss.net/11/22893/2011/> doi:10.5194/acpd-11-22893-2011

- Clement AC, Burgman R, Norris JR (2009) Observational and model evidence for positive low-level cloud feedback. *Science* 325(5939):460. doi:[10.1126/science.1171255](https://doi.org/10.1126/science.1171255)
- Collins WD, Rasch PJ, Boville BA, McCaa JR, Williamson DL, Kiehl JT, Briegleb B, Bitz C, Lin SJ, Zhang M, Dai Y (2004) Description of the NCAR community atmosphere model (CAM 3.0). CGD, TN-464+STR, 214pp
- Colman R (2003) A comparison of climate feedbacks in general circulation models. *Clim Dyn* 20:865–873
- Dee DP et al (2011) The ERA-Interim reanalysis: configuration and performance of the data assimilation system. *Quart J R Meteorol Soc* 137:553–597
- Delworth TL et al (2006) GFDL's CM2 global coupled climate models—part 1: formulation and simulation characteristics. *J Clim* 19:643–674
- Déqué M, Dreveton C, Braun A, Cariolle D (1994) The ARPEGE/IFS atmosphere model: a contribution to the French community climate modelling. *Clim Dyn* 10:249–266
- Donner LJ et al (2011) The dynamical core, physical parameterizations, and basic simulation characteristics of the atmospheric component AM3 of the GFDL Global Coupled Model CM3. *J Clim* 24:3484–3519
- Dufresne JL, Bony S (2008) An assessment of the primary sources of spread of global warming estimates from coupled atmosphere–ocean models. *J Clim* 21:5135–5144
- Dufresne JL et al (2013) Climate change projections using the IPSL-CM5 earth system model: from CMIP3 to CMIP5. *Clim Dyn* 40:2123–2165
- Dunne JP et al (2012) GFDL's ESM2 Global coupled climate carbon earth system models. Part I: physical formulation and baseline simulation characteristics. *J Clim* 25:6646–6665
- Eitzen ZA, Xu KM, Wong T (2011) An estimate of low-cloud feedbacks from variations of cloud radiative and physical properties with sea surface temperature on interannual time scales. *J Clim* 24:1106–1121. doi:[10.1175/2010JCLI3670.1](https://doi.org/10.1175/2010JCLI3670.1)
- Garay MJ, de Szoeke SP, Moroney CM (2008) Comparison of marine stratocumulus cloud top heights in the southeastern Pacific retrieved from satellites with coincident ship-based observations. *J Geophys Res* 113:D18204. doi:[10.1029/2008JD009975](https://doi.org/10.1029/2008JD009975)
- Gordon C et al (2000) The simulation of SST, sea ice extents and ocean heat transports in a version of the Hadley Centre coupled model without flux adjustments. *Clim Dyn* 16:147–168
- Gordon HB et al (2002) The CSIRO Mk3 climate system model. [Electronic publication]. Aspendale: CSIRO Atmospheric Research. (CSIRO Atmospheric Research technical paper; no. 60). 130pp
- Gregory JM, Webb MJ (2008) Tropospheric adjustment induces a cloud component in CO₂ forcing. *J Clim* 21:58–71. doi:[10.1175/2007JCLI1834.1](https://doi.org/10.1175/2007JCLI1834.1)
- Hartmann DL, Ockert-Bell ME, Michelsen ML (1992) The effect of cloud type on earth's energy balance: global analysis. *J Clim* 5:1281–1304
- Hourdin F et al (2006) The LMDZ4 general circulation model: climate performance and sensitivity to parametrized physics with emphasis on tropical convection. *Clim Dyn* 27:787–813. doi:[10.1007/s00382-006-0158-0](https://doi.org/10.1007/s00382-006-0158-0)
- Jakob C (2001) The representation of cloud cover in atmospheric general circulation models. PhD Thesis, Ludwig-Maximilians-Universität, 193pp, available from ECMWF
- King MD, Kaufman Y, Menzel WP, Tanré D (1992) Remote sensing of cloud, aerosol, and water vapor properties from the moderate resolution imaging spectroradiometer (modis). *IEEE Trans Geosci Remote Sens* 30:2–27
- Klein SA, Hartmann DL (1993) The seasonal cycle of low stratiform clouds. *J Clim* 6:1587–1606
- Knutti R, Masson D, Gettelman A (2013) Climate model genealogy: generation CMIP5 and how we got there. *Geophys Res Lett* 40:1194–1199. doi:[10.1002/grl.50256](https://doi.org/10.1002/grl.50256)
- K-1 model developers (2004) K-1 coupled model (MIROC) description, K-1 technical report, 1. In: Hasumi H, Emori S (eds) Center for climate system research, University of Tokyo, 34pp
- Larson K, Hartmann DL, Klein SA (1999) The role of clouds, water vapor, circulation, and boundary layer structure in the sensitivity of the tropical climate. *J Clim* 12:2359–2374
- Lau WM, Ho CH, Chou MD (1996) Water vapor and cloud feedback over tropical oceans: can we use ENSO as a surrogate for climate change?. *Geophys Res Lett* 23:2971–2974
- Liu Z, Vavrus S, He F, Wen N, Zhong Y (2005) Rethinking tropical ocean response to global warming: the enhanced equatorial warming. *J Clim* 18:4684–4700
- Lohmann U, Feichter J (2001) Can the direct and semi-direct aerosol effect compete with the indirect effect on a global scale? *Geophys Res Lett* 28:159–161
- Martin GM et al (2011) The HadGEM2 family of met office unified model climate configurations. *Geosci Model Dev* 4:723–757
- Medeiros B, Stevens B (2011) Revealing differences in GCM representations of low clouds. *Clim Dyn* 36:385–399. doi:[10.1007/s00382-009-0694-5](https://doi.org/10.1007/s00382-009-0694-5)
- Medeiros B, Stevens B, Held IM, Zhao M, Williamson DL, Olson JG, Bretherton CS (2008) Aquaplanets, climate sensitivity, and low clouds. *J Clim* 21:4974–4991
- Miller RL (1997) Tropical thermostats and low cloud cover. *J Clim* 10:409–440
- Mitchell JFB, Senior CA, Ingram WJ (1989) CO₂ and climate: a missing feedback?. *Nature*, 341:132–134
- Moeng CH, Stevens B (2000) Marine stratocumulus and its representation in GCMs. Book chapter on general circulation model development: past, present, and future, proceedings of a symposium in honor of Professor Akio Arakawa. Ed. D.A. Randall, Published by Academic Press, 807pp
- Nakićenović N et al (2000) IPCC Special report on emissions scenarios. Cambridge University Press, Cambridge
- Neale RB et al (2010) Description of the NCAR community atmosphere model (CAM 4.0). Technical Report, NCAR
- Norris JR (2001) Has northern Indian Ocean Cloud cover changed due to increasing anthropogenic aerosol?. *Geophys Res Lett* 28:3271–3274. doi:[10.1029/2001GL013547](https://doi.org/10.1029/2001GL013547)
- Reynolds RW, Rayner NA, Smith TM, Stokes DC, Wang W (2002) An improved in situ and satellite SST analysis for climate. *J Clim* 15:1609–1625
- Rieck M, Nuijens L, Stevens B (2012) Marine boundary layer cloud feedbacks in a constant relative humidity atmosphere. *J Atmos Sci* 69:2538–2550
- Roeckner E et al (1996) The atmospheric general circulation model ECHAM-4: model description and simulation of present-day climate. Reports of the Max-Planck-Institute, Hamburg, No. 218, 90pp
- Roeckner E et al (2003) The atmospheric general circulation model ECHAM5. Part I: model description. Max Planck Institute for Meteorology Rep. 349, 127pp
- Rossow WB, Schiffer RA (1991) ISCCP cloud data products. *Bull Am Meteorol Soc* 72:2–20
- Rotstayn LD, Collier MA, Dix MR, Feng Y, Gordon HB, O'Farrell SP, Smith IN, Syktus J (2010) Improved simulation of Australian climate and ENSO-related rainfall variability in a global climate model with an interactive aerosol treatment. *Int J Climatol* 30:1067–1088. doi:[10.1002/joc.1952](https://doi.org/10.1002/joc.1952)
- Schmidt GA et al (2006) Present-day atmospheric simulations Using GISS ModelE: comparison to in situ, satellite, and reanalysis data. *J Clim* 19:153–192

- Schmidt GA et al (2013) Configuration and assessment of the GISS ModelE2 contributions to the CMIP5 archive. *J Adv Model Earth Syst* (submitted)
- Scinocca JF, McFarlane NA, Lazare M, Li J, Plummer D (2008) Technical Note: the CCCma third generation AGCM and its extension into the middle atmosphere. *Atmos Chem Phys* 8:7055–7074
- Senior CA, Mitchell JFB (1993) Carbon dioxide and climate: the impact of cloud parameterization. *J Clim* 6:393–418
- Slingo A (1990) Sensitivity of the earth's radiation budget to changes in low clouds. *Nature* 343:49–51
- Slingo JM (1980) A cloud parameterization scheme derived from GATE data for use with a numerical model. *Quart J Roy Meteorol Soc* 106:747–770
- Slingo JM (1987) The development and verification of a cloud prediction scheme for the ECMWF model. *Quart J R Meteorol Soc* 113:899–927
- Soden BJ, Held IM (2006) An assessment of climate feedbacks in coupled ocean-atmosphere models. *J Clim* 19:3354–3360
- Soden BJ, Vecchi GA (2011) The vertical distribution of cloud feedback in coupled ocean-atmosphere models. *Geophys Res Lett* 38:L12704. doi:10.1029/2011GL047632
- Stephens GL (2005) Cloud feedbacks in the climate system: a critical review. *J Clim* 18:237–273
- Stevens B et al (2013) The atmospheric component of the MPI-M Earth System Model: ECHAM6. *J Adv Model Earth Syst* 5:146–172
- Sun F, Hall A, Qu X (2011) On the relationship between low cloud variability and lower tropospheric stability in the Southeast Pacific. *Atmos Chem Phys* 11:9053–9065. doi:10.5194/acp-11-9053-2011
- Sutton RT, Dong B, Gregory JM (2007) Land/sea warming ratio in response to climate change: IPCC AR4 model results and comparison with observations. *Geophys Res Lett* 34:L02701. doi:10.1029/2006GL028164
- Taylor KE, Stouffer RJ, Meehl GA (2012) An overview of CMIP5 and the experiment design. *Bull Am Meteorol Soc* 93:485–498
- Tiedtke M (1993) Representation of clouds in large-scale models. *Mon Wea Rev* 121:3040–3061
- Vecchi GA, Soden BJ, Wittenberg AT, Held IM, Leetmaa A, Harrison MJ (2006) Weakening of tropical Pacific atmospheric circulation due to anthropogenic forcing. *Nature* 441. doi:10.1038/nature04744
- Volodin EM, Diansky NA (2004) El-Nino reproduction in coupled general circulation model of atmosphere and ocean. *Russian Meteorol Hydrol* 12:5–14
- Washington WM et al (2000) Parallel climate model (PCM) control and transient simulations. *Clim Dyn* 16:755–774
- Watanabe M, Emori S, Satoh M, Miura H (2009) A PDF-based hybrid prognostic cloud scheme for general circulation models. *Clim Dyn* 33:795–816
- Watanabe M et al (2010) Improved climate simulation by MIROC5: mean states, variability, and climate sensitivity. *J Clim* 23:6312–6335
- Watanabe S et al (2011) MIROC-ESM: model description and basic results of CMIP5-20c3m experiments. *Geosci Model Dev Discuss* 4:1063–1128. doi:10.5194/gmdd-4-1063-2011
- Watanabe M et al (2012) Fast and slow timescales in the tropical low-cloud response to increasing CO₂ in two climate models. *Clim Dyn* 39:1627–1641. doi:10.1007/s00382-011-1178-y
- Weaver CP, Ramanathan V (1997) Relationships between large-scale vertical velocity, static stability, and cloud radiative forcing over northern hemisphere extratropical oceans. *J Clim* 10:2871–2887
- Webb MJ et al (2006) On the contribution of local feedback mechanisms to the range of climate sensitivity in two GCM ensembles. *Clim Dyn* 27:17–38
- Webb MJ, Lambert FH, Gregory JM (2012) Origins of differences in climate sensitivity, forcing and feedback in climate models. *Clim Dyn*. doi:201210.1007/s00382-012-1336-x
- Williams KD, Ringer M, Senior C (2003) On evaluating cloud feedback: comparing the response to increased greenhouse gases with current climate variability. *Clim Dyn* 20:705–721
- Williams KD et al (2006) Evaluation of a component of the cloud response to climate change in an intercomparison of climate models. *Clim Dyn* 26:145–165
- Wood R, Bretherton CS (2006) On the relationship between stratiform low cloud cover and lower-tropospheric stability. *J Clim* 19:6425–6432
- Wu T et al (2010) The Beijing climate center atmospheric general circulation model: description and its performance for the present-day climate. *Clim Dyn* 34:123–147. doi:10.1007/s00382-008-0487-2
- Wyant MC, Khairoutdinov M, Bretherton CS (2006) Climate sensitivity and cloud response of a GCM with a superparameterization. *Geophys Res Lett* 33:L06714. doi:10.1029/2005GL025464
- Yao MS, Del Genio AD (1999) Effects of cloud parameterization on the simulation of climate changes in the GISS GCM. *J Clim* 12:761–779
- Yu Y, Zhang X, Guo Y (2004) Global coupled ocean-atmosphere general circulation models in LASG/IAP. *Adv Atmos Sci* 21:444–455
- Yukimoto S et al (2001) The new meteorological research institute coupled GCM (MRI-CGCM2): model climate and variability. *Meteorol Geophys* 51:47–88
- Yukimoto S et al (2011) Meteorological Research Institute-Earth System Model Version 1 (MRI-ESM1): model description. Technical Report of the Meteorological Research Institute, 64, 83pp
- Zhang MH, Bretherton C (2008) Mechanisms of low cloud-climate feedback in idealized single-column simulations with the community atmospheric model, version 3 (CAM3). *J Clim* 21:4859–4878
- Zelinka MD, Klein SA, Hartmann DL (2012) Computing and partitioning cloud feedbacks using cloud property histograms. Part II: attribution to changes in cloud amount, altitude, and optical depth. *J Clim* 25:3736–3754